

IN VIVO DIFFUSE REFLECTANCE SPECTROSCOPY
OF HUMAN TISSUE

FROM POINT MEASUREMENTS TO IMAGING

ERIK HÄGGBLAD



Linköping University
INSTITUTE OF TECHNOLOGY

Department of Biomedical Engineering
Linköpings universitet
Linköping 2008

Linköping Studies in Science and Technology. Dissertations, No. 1210

Author:

Erik Häggblad

Department of Biomedical Engineering

Linköping University

SE-581 85 Linköping, Sweden

Illustrations:

Erik Häggblad, unless otherwise noted.

Layout:

Erik Häggblad

Copyright © 2008 Erik Häggblad, unless otherwise noted.

All rights reserved.

Erik Häggblad

In Vivo Diffuse Reflectance Spectroscopy of Human Tissue:
From Point Measurements to Imaging

ISBN 978-91-7393-809-9

ISSN 0345-7524

Printed in Sweden by LiU-Tryck, Linköping, 2008

“All of us are watchers,
of television, of time clocks,
of traffic on the freeway,
but few are observers.

Everyone is looking, not many are seeing.”

Peter Leschak

ABSTRACT

This thesis presents the non-invasive use of diffuse reflectance spectroscopy (DRS) to provide information about the biochemical composition of living tissue. During DRS measurements, the incident, visible light is partially absorbed by chromophores but also scattered in the tissue before being remitted.

Human skin and heart, the main tissue objects in this thesis, are dependent on a sufficient inflow of oxygenized blood, and outflow of metabolic byproducts. This process could be monitored by DRS using the spectral fingerprints of the most important tissue chromophores, oxyhemoglobin and deoxyhemoglobin.

The Beer-Lambert law was used to produce models for the DRS and has thus been a foundation for the analyses throughout this work. Decomposition into the different chromophores was performed using least square fitting and tabulated data for chromophore absorptivity.

These techniques were used to study skin tissue erythema induced by a provocation of an applied heat load on EMLA-treated skin. The absorbance differences, attributed to changes in the hemoglobin concentrations, were examined and found to be related to, foremost, an increase in oxyhemoglobin.

To estimate UV-induced border zones between provoked and non-provoked tissue a modified Beer-Lambert model, approximating the scattering effects, was used. An increase of chromophore content of more than two standard deviations above mean indicated responsive tissue. The analysis revealed an edge with a rather diffuse border, contradictory to the irradiation pattern.

Measuring in the operating theater, on the heart, it was necessary to calculate absolute chromophore values in order to assess the state of the myocardium. Therefore, a light transport model accounting for the optical properties, and a calibrated probe, was adopted and used. The absolute values and fractions of the chromophores could then be compared between sites and individuals, despite any difference of the optical properties in the tissue.

A hyperspectral imaging system was developed to visualize the spatial distribution of chromophores related to UV-provocations. A modified Beer-Lambert approximation was used including the chromophores and a baseline as an approximate scattering effect. The increase in chromophore content was estimated and evaluated over 336 hours.

In conclusion, advancing from a restricted Beer-Lambert model, into a model estimating the tissue optical properties, chromophore estimation algorithms have been refined progressively. This has allowed advancement from relative chromophore analysis to absolute values, enabling precise comparisons and good prediction of physiological conditions.

LIST OF PUBLICATIONS

This thesis is based on the following papers, which are referred to in the text by their Roman numerals. Published papers are reprinted with granted permission from the respective publishers.

- I** Reflection Spectroscopy of Analgesized Skin
Erik Häggblad, Marcus Larsson, Mikael Arildsson,
Tomas Strömberg, and E. Göran Salerud

Microvascular Research, Vol 26, Issue 3, November 2001,
Pages 392-400, Elsevier Limited, Oxford, England.
- II** A Diffuse Reflectance Spectroscopic Study
of UV-Induced Erythematous Reaction
Across Well-Defined Borders in Human Skin
Erik Häggblad, Henrik Petersson, Michail A. Ilias,
Chris D. Anderson and E. Göran Salerud

In manuscript.
- III** Myocardial Tissue Oxygenation Estimated
With Calibrated Diffuse Reflectance Spectroscopy
During Coronary Artery Bypass Grafting
Erik Häggblad, Tobias Lindbergh, M. G. Daniel Karlsson,
Henrik Casimir-Ahn, E. Göran Salerud, and Tomas Strömberg

Journal of Biomedical Optics, Vol 13, Issue 5, September/October 2008,
054030, The International Society of Optical Engineering - SPIE, USA.
- IV** Visible, Hyperspectral Imaging Evaluating
the Cutaneous Response to Ultraviolet Radiation
Michail A. Ilias, Erik Häggblad, Chris Anderson, and
E. Göran Salerud

Proceedings of SPIE - Imaging, Manipulation, and Analysis
of Biomolecules, Cells, and Tissues V, Edited by Daniel L. Farkas;
Robert C. Leif; Dan V. Nicolau, 13 February 2007, Vol. 6441,
644103, The International Society of Optical Engineering - SPIE, USA.

ABBREVIATIONS

ALA	Aminolevulinic acid
AOTF	Acousto-optic tunable filters
AV	Arteriovenous
BaSO ₄	Barium sulphate
CABG	Coronary artery bypass grafting
CCD	Charge-coupled device
CIE	Commission internationale de l'Eclairage
CIElab	Color space defined by CIE
DRS	Diffuse reflectance spectroscopy
FOV	Field of view
FWHM	Full width at half maximum
HSI	Hyperspectral imaging
LCTF	Liquid crystal tunable filter
LDF	Laser Doppler flowmetry
LDPI	Laser Doppler imaging
LDPM	Laser Doppler monitoring
LED	Light emitting diode
MED	Minimal erythema dose
NIR	Near Infrared radiation
OCT	Optical coherence tomography
OPS	Orthogonal polarized spectral imaging
PDT	Photodynamic therapy
PMS	Photon migration spectroscopy
PPG	Photoplethysmography
PpIX	Protoporphyrin IX (nine)
PTFE	Polytetrafluoroethylene
ROI	Region of interest
SDF	Sidestream dark field microscopy
SNR	Signal-to-noise ratio
UV	Ultraviolet

CONTENTS

INTRODUCTION	1
THE LIVING TISSUE	3
MICROCIRCULATION AND BLOOD	3
THE SKIN	5
THE HEART	7
SPECTROSCOPY.....	11
SPECTROMETERS AND MEASUREMENTS	12
LIGHT SOURCES	15
OTHER SPECTROSCOPIC TECHNIQUES	15
ADDITIONAL TECHNIQUES	17
OPTICAL PROPERTIES	21
LIGHT TRANSPORT IN TISSUE.....	22
REFRACTIVE INDEX	23
ABSORPTION.....	24
SCATTERING	25
CHROMOPHORES.....	27
HEMOGLOBIN	28
MYOGLOBIN	30
CYTOCHROMES	31
BILIRUBIN	31
MELANIN	32
CAROTENOIDS	33
LIPIDS	34
WATER	34
ADDITIONAL CHROMOPHORES.....	35
AIMS OF THE THESIS	37
SPECTROSCOPY AS APPLIED IN THE THESIS	39
PREPROCESSING OF SPECTRA	40
DIFFERENCE SPECTRA.....	41
SPECTROSCOPIC MODELS	42
CURVE FITTING.....	45
ASSESSING THE CURVE FIT	46
HYPERSPECTRAL IMAGING	49
GENERAL ASPECTS	49
THE HARDWARE.....	50
NORMALIZATION.....	52
SOFTWARE AND ANALYSIS	53
EVALUATION OF THE SYSTEM	54
RESULTS AND REVIEW OF THE PAPERS	57
PAPER I: REFLECTION SPECTROSCOPY OF ANALGESIZED SKIN.....	57
PAPER II: A DIFFUSE REFLECTANCE SPECTROSCOPIC STUDY OF UV-INDUCED ERYTHEMATOUS REACTION ACROSS WELL-DEFINED BORDERS IN HUMAN SKIN	59
PAPER III: MYOCARDIAL TISSUE OXYGENATION ESTIMATED WITH CALIBRATED DIFFUSE REFLECTANCE SPECTROSCOPY DURING CORONARY ARTERY BYPASS GRAFTING	62
PAPER IV: VISIBLE, HYPERSPECTRAL IMAGING EVALUATING THE CUTANEOUS RESPONSE TO ULTRAVIOLET RADIATION.....	64
DISCUSSION AND CONCLUSIONS	67
METHODOLOGICAL AND MODEL CONSIDERATIONS.....	67
PHYSIOLOGICAL ASPECTS	72
FUTURE DIRECTIONS.....	74
CONCLUSION	74
ACKNOWLEDGMENTS	77
REFERENCES	79

“The color of the skin, to a certain extent, serves as an index of the state of well-being, or the converse, and has been interpreted, after various modes and manners of expression, as evidence of health or disease.”

Sheard and Brunstig, 1929

1

*“...I procured me a Triangular glass Prisme
to see therewith
the celebrated Phaenomena of Colours.”
Isaac Newton*

INTRODUCTION

The origin of this thesis is the interaction of light with tissue molecules and how it is possible to predict and model these interactions in order to use the results to characterize and diagnose tissue.

The living tissue is highly dependent on a sufficient inflow of nutritive blood carrying oxygen, and an outflow of metabolic byproducts¹. If this demand is not met the tissue will suffer, stop functioning and eventually die².

To determine the condition of a tissue and to diagnose diseases, clinicians use visual perception of tissue color on a daily basis. The eye can, however, only judge the appearance of color but not interpret the underlying reasons for this appearance. Therefore the eye is easily deceived, resulting in subjective judgment. Since human vision lacks the ability to interpret the wavelength dependence of color, techniques for measuring light with a high wavelength resolution are necessary to support the identification of tissue chromophores with a high specificity and sensitivity. Preferably, these techniques should be performed in both experimental and clinical settings to be able to quantify both spatial and temporal changes of the identified chromophores.

The main principle of spectral observations, or spectroscopy, was demonstrated and documented in 1672 by Isaac Newton who showed the existence of the spectrum of light by using a prism and noticing dispersion of white light into separate colors³. Among the historical milestones leading to the contemporary use of

spectroscopy in medicine and biology, Hoppe's findings in 1862 concerning light absorption characteristics of hemoglobin⁴, and Stokes' studies in 1864 on the effects of oxygenation changes in hemoglobin, are of special importance. The ideas in their original works were implemented, as early as in the beginning of the 20th century, in the spectroscopic studies on the pigmentation of human skin for diagnostic purposes^{5,6}.

Since then, the capacity of the technique has been extensively tested in a variety of biomedical applications⁶⁻⁹. The specific implementation of the technique measuring diffusely reflected light, diffuse reflectance spectroscopy (DRS), can be regarded as being a port or window, through which information on deeper tissue processes and organ functions can be mirrored and made accessible for observation and analysis. Simultaneously, DRS reflects the influence of environmental and internal processes acting on the biological system.

During DRS measurements, the identification of chromophores in a living system is possible by analyzing the characteristic fingerprints, or spectral signatures, at the detector output when compared to a spectroscopic reference.

This thesis focuses on the use of diffuse reflectance spectroscopy on human tissue *in vivo*. The aim was to develop and evaluate diffuse reflectance spectroscopy techniques for assessing tissue chromophores related to oxygenation and pigmentation.

2

*"When humans visualize a body,
they see mostly the skin."
Nina G. Jablonski, 2004*

THE LIVING TISSUE

In this chapter a short overview of relevant tissues will be presented. To begin with the microcirculation is presented structurally as well as the circulation in a general perspective. The subsequent text will cover the skin and the heart in more detail.

MICROCIRCULATION AND BLOOD

Throughout the body an intricate system of blood vessels can be found, starting with the aorta and thereafter the arteries that bifurcate throughout the body to lead to the microvasculature. The circulatory system is completed by the venules and veins leading back to the heart. The purpose of the circulatory system is to distribute and regulate blood flow throughout the body to support the various nutritional needs of the different tissues.^{10, 11}

Conventionally the structural microcirculation is defined as the smallest vessels in the body including the arterioles (\varnothing 20-50 μm), metarterioles (\varnothing 10-15 μm), capillaries (\varnothing 4-10 μm), arteriovenous (AV, \varnothing ~40 μm) shunts, and venules (\varnothing ~50 μm)^{11, 12}. The microvasculature can be found everywhere in the body with the number of vessels largely depending on the nutritional needs of the actual tissue¹⁰. However, the AV-shunts foremost can be found in the extremities and the hands and feet¹¹. The purpose of the microcirculatory networks is to distribute the blood flow as close as possible to single cells^{11, 12}. Thus, the microcirculation can be functionally defined as the body's nutritive vessels.

To regulate the blood flow all the vessels, except for the capillaries, have smooth muscle cells surrounding the lumen. This musculature, which is controlled by the autonomic nervous system and chemical compounds in the blood, can constrict and dilate the vessel lumen to direct and regulate the flow as needed. In addition the blood flow through the individual capillaries can be stemmed by small single muscles called precapillary sphincters.^{11, 12}

To facilitate nutritional exchange at the cellular level, the capillaries are reduced in diameter with the smallest vessels having a diameter which forces the erythrocytes to slowly squeeze through one by one at low speeds. Furthermore the capillary wall consists of a single layer of endothelial cells in order to facilitate transport of oxygen and nutrients over the vessel wall.¹²

The microcirculatory flow has two essential tasks: the transport of oxygen and nutrition to the cells and the transport of metabolic byproducts from the cells so that the tissue can function properly¹². The circulating blood emanates from the heart, is oxygenized in the lungs, flows out into the body and progresses towards the capillary networks where most of the exchange between blood and cells is conducted. The flow at the capillary level does not always present a pulsatile flow which is normally encountered in the larger vessels on the arterial side. Instead a flow pattern with the erythrocytes moving intermittently can be observed at times. A general direction of the movement of erythrocytes can be identified emanating from the arterioles and ending at the venules, but there is no physical restriction of the movement and erythrocytes can thus move backwards as well. The AV-shunts that do not partake in the nutritional flow can, e.g. for thermoregulatory reasons, bypass the flow through the capillaries and canalize the flow directly to the venous side which causes total absence of blood in the capillaries^{11, 12}.

Absence of blood in the capillaries is however nothing unexpected due to the intermittent flow. Further, not all capillaries are perfused at once but are emptied or collapsed for periods of time, especially in areas where the nutritional demand is moderate or low. In fact, most tissues have an excess capacity of up to 400% compared to normal conditions. For tissues such as muscles, as few as 5% of the capillaries are open during resting conditions¹². An abnormal reduction or loss of capillary flow, ischemia, or oxygen content, below the tissue demand can lead to local anoxia, and acidosis and a prolonged absence of flow can even result in necrosis despite normal arterial flow^{2, 12}. In contrast, an increase of the nutritional demand will lead to an increase of the microcirculatory flow. Prolonged

demand will lead to a higher capillary flow and oxygen extraction and eventually angiogenesis^{2, 11}.

The blood that circulates in the vessels consists mainly of plasma and erythrocytes with the ratio of erythrocytes per volume of blood being called hematocrit¹³. Normal values can be found for the hematocrit between 0.37-0.54 for adults¹⁴, but since the amount of plasma varies the hematocrit will also vary depending on where in the vascular system it is measured. For example in the capillaries, wherein a fifth of the total blood volume can be found, a lower hematocrit value can be expected due to a lower number of erythrocytes¹³. The erythrocytes in themselves are biconcave discs with an approximate diameter of 7-8 μm . About 33% of the cell weight consists of the oxygen binding hemoglobin molecules¹⁰. Arterial blood contains 90-95% oxyhemoglobin and venous blood contains normally less than 53%. Values in between these numbers can be found in the capillaries¹⁴.

THE SKIN

The skin, the cutis, is the largest organ of the human body and it is responsible for a number of tasks such as protecting the inside of the body from the sometimes harmful environment in which humans live. The skin structure varies for different body sites with a main differentiation being found between thick hairless skin and thinner hairy skin. Apart from the regional differences there also exist inter-individual differences in the skin, for example regarding the thickness, vascularity, pigmentation and the frequency of inherent appendages¹⁵.

In general, the skin is a layered structure with two main reactive layers, the epidermis and the dermis, see Figure 1. The stratified epidermis can be further divided into the stratum corneum, stratum lucidum, stratum granulosum, stratum spinosum, and stratum basale; all representing different degrees of differentiation of keratinocytes. Other constituents that are of interest in epidermis are the melanocytes and melanin granules. The combined thickness of epidermis varies in the range of 48-170 μm . The stratum corneum, the outermost layer, has a thickness of about 8-20 μm but can be up to 10 times thicker on the palms and soles^{15, 16}.

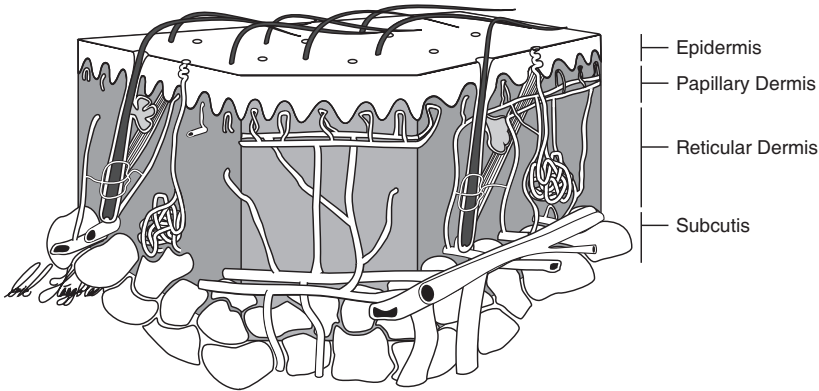


Figure 1: Schematic drawing of a skin section depicting the different layers. The middle section shows the approximation usually made in bio-optical applications with a superficial plexus and a deeper plexus; capillaries are only drawn in the papillary dermis but can also be found in the dermis. The flanking sides of the middle section show some of the complexity of the skin with appendages such as hair follicles and different glands; figure not drawn to scale.

The junction between the two skin layers constitutes a corrugated segment, the papillary region. The superficial, papillary dermis contains loosely organized tissue and fine elastic fibers. The reticular layer below is mainly composed of dense, irregular connective tissue as well as collagen, elastic fibers and a small amount of adipose tissue.¹⁰

The dermis also embraces inherent functional appendages such as hair follicles, hairs (\varnothing 30-120 μm) and the associated erector muscle, different nerves and nerve endings, sebaceous glands and sweat glands (\varnothing 20-50 μm). The total thickness of dermis is in the range of 1-4 mm.¹⁶

The dermis is connected via protruding fibers extending into the deeper lying subcutis, which mainly constitutes adipose and loose connective tissue¹⁰. The subcutaneous adipocytes are arranged in lobules (\varnothing ~50 μm) separated by loose connective tissue forming compartments that allow for vessels and nerve fibers to pass to the upper layers¹⁶.

The microvasculature in the skin is usually described as being arranged in two main plexuses of larger vessels, the superficial plexus immediately underneath the epidermis and the deeper lying plexus at the dermis-subcutaneous junction. In the dermal part of the papillary region end loop capillaries can be found that give nutritive flow to the lower regions of the epidermis. In this region approximately one capillary can be found per papilla in order to meet the high nutritional demand of the stratum granulosum. The capillary density of the papillary layer can be up to 70 capillaries

per mm².¹⁷ The papillary capillaries ascend from the superficial plexus which is a horizontal network of arterioles and venules in the papillary dermis. In the border zone of the reticular dermis and subcutis the deeper lying plexus can be found. This layer is formed by larger arterioles and veins protruding from the subcutaneous tissue. Branching arterioles and venules interconnect the two plexuses and in addition lateral capillaries interconnect between them to supply hair follicles, glands and erector muscles with blood. Compared to the well-perfused dermis, vessels in the subcutis are relatively scarce. The large arteries supplying the skin plexuses and large venules can however be found¹⁵.

THE HEART

Not much larger than a closed fist, the heart muscle is responsible for keeping the human body alive by having enough capacity to pump life-giving blood to the cells throughout the body.

The heart is a muscle with a complex three dimensional helix structure situated inside the pericardium^{10, 18}. The heart in itself has three layers including the epicardium followed by the cardiac muscle, the myocardium, and the innermost layer covered by a layer of epithelial cells, the endocardium¹⁰, see Figure 2.

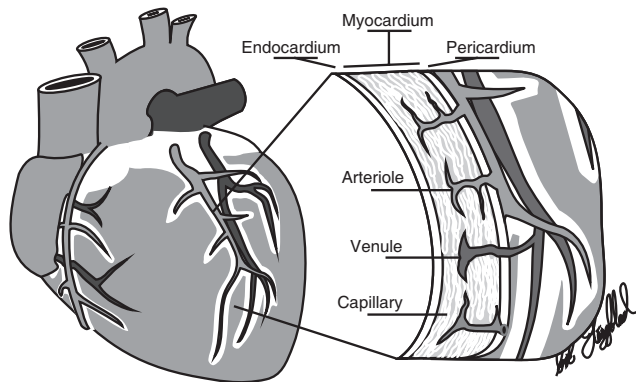


Figure 2: Schematic overview of the heart and a cross section of the heart wall, depicting the different layers and the microcirculatory vasculature; figure not drawn to scale.

The myocardium constituting the major part of the heart consists to a large extent of muscle fibers, the myocytes, and capillaries but also of connective tissue which forms the interstitium. The fractional volume of myocytes is about 70% of the heart volume, but myocytes only account for a one-third of the total number of cells, the rest constitute various smaller nonmyocytic cells^{19, 20}. In addition to the muscle fibers and connective tissue there also exist cell structures related to

electrical and endocrine functions of the heart, e.g. the Purkinje fibers and the subendocardial lymphatic channels^{20, 21}.

The heart surface can be partially covered with epicardial fat, e.g. around the main coronary arteries and the larger branches, which obscures the myocardium and other structures; the total amount and thickness of the fat is largely related to total body fat and age¹⁸.

The total thickness of the myocardium varies with location from approximately 2 mm in the septum to 15 mm of the left ventricle²¹. The epicardium is a thinner layer that consists of collagen fibers and a layer of endothelial cells. The endocardium consists of a thin layer of collagen and endothelial cells which has a thickness of a few cell layers^{10, 21}.

The vasculature of the heart muscle originates from the aortic root with the right and the left coronary arteries. The arteries situated on the epicardial surface encircle the heart and gradually branch into smaller vessels which protrude into the myocardium^{21, 22}. At the epicardial level anastomoses between the coronary vessels exist²¹. Arteries can then be found penetrating the myocardium bifurcating into arterioles and metarterioles to finally form the capillaries^{21, 22}. Venules and veins then drain the capillaries through arcading vessels where more than one vein can be associated with each region supported by a single artery²². A small number of veins drain right into the heart cavities whereas most blood drainage occurs through the coronary sinus²².

The capillaries of the heart closely follow the individual muscle fibers and have a structure with end-capillary loops which can form arcade like structures where new loops emerge at the apex of former loops. The capillary structure of different arteriole origins can be interleaved but has no significant overlap between separate branches of capillaries. In contrast to the frequent epicardial anastomoses there is no evidence that any anastomoses exist at the capillary level.²³

To meet the continuously high oxygen demand of the heart it has a high capillary density with a ratio of approximately one capillary per myocyte²¹. This translates into a value of 3000-4000 capillaries per mm² in the pig heart and approximately 90% of the myocardial blood volume can be found in those capillaries²².

To regulate the blood flow in the extensive capillary net precapillary sphincters also exist in the heart which can shut off blood flow completely. This will make the microcirculatory flow vary, both spatially and temporally²¹. It has been estimated that only 50% of the capillaries are perfused at once during resting conditions, but an increase of the workload will, however, increase this number

rapidly²². The contractile movements of the heart make the blood flow complex with interactions between the vessels and the contracting muscle fibers, resulting in a unique flow pattern where the arterial flow is generally diastolic and venous flow systolic²⁴.

3

"Many eyes go through the meadow,
but few see the flowers in it."
Ralph Waldo Emerson

SPECTROSCOPY

Spectroscopy[†] is the generalized study of chemical structures and dynamics of a sample by way of the absorption, emission, and scattering of electromagnetic radiation. A *spectrometer* is an apparatus able to measure and record the intensity per wavelength, wavenumber or frequency. In accordance with previous definitions a *spectrum* (plural *spectra*) is a registration of the electromagnetic distribution against the chosen photon characteristics. The general class of spectroscopy is thoroughly widespread and is applied in areas such as chemistry, astronomy, and biomedical engineering. Spectroscopic principles are valid throughout most of the electromagnetic spectra which includes X-rays, radio waves and heat waves.⁵

The common denominator for the spectroscopic applications is the possibility to differentiate and study chemical structures or compositions by their characteristic absorption which varies with wavelength, i.e. the "chemical fingerprints". This thesis focuses on the use of diffuse reflectance spectroscopy in biomedical applications and the absorption of light in the tissue. It is further restricted towards a small part of the electromagnetic radiation that is characterized as optical radiation, i.e. the wavelength range that stretches from ultraviolet (UV) radiation to infrared radiation with a specific focus on visible light, see Figure 3.

[†] From Latin: *Spectrum* – apparition, and Greek: *skopein* – to view.

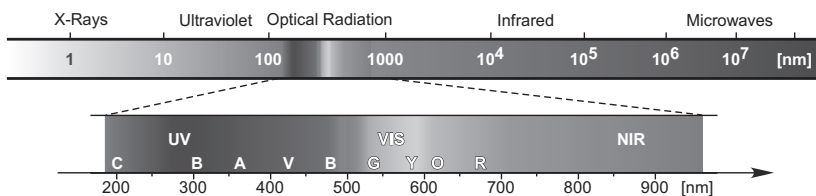


Figure 3: Optical radiation and visible light is just a small portion of the whole electromagnetic spectrum, which includes X-rays, radio waves and heat waves, UV = Ultraviolet radiation (C, B and A); VIS = Visible light, (Violet, Blue, Green, Yellow, Orange, and Red); NIR = Near infrared radiation.

Spectroscopy can provide detailed information about the underlying biochemical composition of a tissue. Incident light can be partially absorbed by endogenous but also exogenous chromophores and it is scattered by the cells, organelles, and fibers present. The resultant light which is backscattered and remitted from the tissue is then recorded for spectral analysis. This is especially appealing since many of the important substances that interact with light are also necessary for the well-being of the tissue, e.g. hemoglobin. The non-invasive approach, the harmless use of light, and the possibility of real time measurements can be considered as major benefits for diagnosis of living tissue. Finally, the use of light does not affect the measurement situation itself. These aspects make it possible to study the microcirculation non-invasively without affecting the tissue; something that is important since any provocation of the tissue can result in a measurement of the provocation effect rather than the condition of the tissue itself.

SPECTROMETERS AND MEASUREMENTS

There are many different types of spectrometers, but the working principle of each apparatus is basically the same. This section describes the working principle of spectrometers with DRS as a basis. The basic configuration of a spectroscopic setup is based on a light source, delivering and collecting optics, a dispersive element, and a detector, see Figure 4. The light source, which preferably has known emission properties, is used to illuminate a sample under study. The incident light is affected and modified spectrally by the sample's ability to attenuate the light which depends upon the mixture as well as the inherent structure of the sample. The sample can be illuminated using wave guides or optical components; likewise the remitted light can be captured by fiber optics²⁵, integrating spheres²⁶ or collecting optics²⁷. The remitted light is directed to the dispersive element where the light is split into separate wavelength components and recorded by a suitable detector. By studying and comparing the remitted light intensity with the incident light intensity it is possible

to make estimations about the biochemical contents and the properties of the sample^{5, 28}.

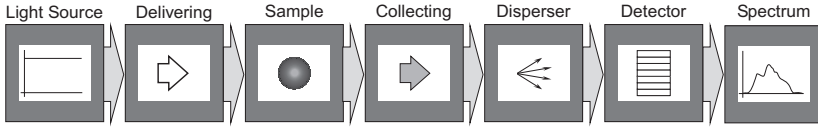


Figure 4: Overview of the basic principle of a spectrometer: A light source illuminates a sample with which the light interacts, the remitted light from the sample is then collected, dispersed and recorded by the spectrometer yielding a spectrum.

To monitor the illuminating light characteristics and the components of the system a reference recording of incident light intensity, I_0 [counts], should be performed. This is usually realized using a reference sample with known scattering and absorbing properties. The white reference is often a tile of barium sulphate (BaSO_4) or a plastic tile of polytetrafluoroethylene (PTFE), which both have a reflectivity of almost 100% throughout the visible light range. In addition to high and uniform reflectivity, an eligible aspect is that the reference should be time invariant.²⁶

The recorded remitted intensity, I , can then be compensated by relating the recorded signal from the sample to the reference spectra and thereby minimizing the influence from the system. To further compensate for the system, e.g. the detector, but also for stray light that may contaminate the signal, a background spectrum, B , can be recorded in absence of the light source. The resultant compensation, or normalization, is conventionally performed by calculating the reflectance, R , of a sample as a function of wavelength, λ [nm], as:

$$\text{Eq. 1} \quad R(\lambda) = \left(\frac{I_o(\lambda) - B_o(\lambda)}{I(\lambda) - B(\lambda)} \right).$$

Depending on the application the transmittance, T , can be calculated analogously to the reflectance.

The intensity profile of the background spectrum, B , can be neglected whenever the recorded intensity for I and I_0 is much higher than B , but it can prove crucial for weaker reflectance spectra, which otherwise can give an unacceptably low signal-to-noise ratio (SNR).

The absorbance, A , which gives the absorbing characteristics of the sample, can thereby be calculated as:

$$\text{Eq. 2} \quad A(\lambda) = -\log(R(\lambda)) = \log \left(\frac{I_o(\lambda) - B_o(\lambda)}{I(\lambda) - B(\lambda)} \right) = \log \left(\frac{I_o(\lambda)}{I(\lambda)} \right)_{B=0}.$$

The intensity of light in a sample decreases exponentially with the molar absorptivity, $\varepsilon(\lambda)$ [ml/(g·mm) or L/(mmol·mm)], concentration, C [g/ml or mmol/L], and the pathlength, l [mm]. This relationship is commonly known as the Beer-Lambert law and by convention it is defined as:

$$\text{Eq. 3} \quad I(\lambda) = I_0(\lambda) \cdot e^{-\varepsilon(\lambda) \cdot C \cdot l}.$$

The Beer-Lambert law is strictly only valid if three assumptions are made²⁹. The first is that the light should be monochromatic, in the aspect that different wavelengths should not interfere with each other. The second regards the actual pathlength of the photons which should be unique and known, e.g. measurement through a cuvette with an absorber but without any scattering particles. Presence of scattering particles will change the actual pathlength and thereby also affect the apparent absorbance. Since scattering varies with wavelength, the pathlength will also be wavelength dependent. The third and final assumption is that if two or more absorbers are present their absorption processes should be independent which is described by following equation:

$$\text{Eq. 4} \quad I(\lambda) = I_0(\lambda) \cdot e^{-(\varepsilon_1(\lambda)C_1 + \varepsilon_2(\lambda)C_2 + \dots + \varepsilon_m(\lambda)C_m)l}.$$

Using Equation 2 to 4 it is rudimentary to derive an equation to relate the recorded absorbance to the constituents of the sample, which is defined by the alternative formulation of Beer-Lambert law using the conversion factor of $\ln(10)$ which is sometimes omitted³⁰:

$$\text{Eq. 5} \quad A(\lambda) = \ln(10) \varepsilon(\lambda) \cdot C \cdot l = 2.3026 \cdot \sum_i \varepsilon_i(\lambda) \cdot C_i \cdot l.$$

The absorbance can also be described by using the absorption coefficient μ_a [mm⁻¹], which is proportional to the concentration of the absorbers and their extinction coefficients as:

$$\text{Eq. 6} \quad A(\lambda) = \mu_a(\lambda) \cdot l = 2.3026 \cdot \varepsilon(\lambda) \cdot C \cdot l.$$

Despite the limiting assumptions for the Beer-Lambert law, originally developed for transmission, it is the basis for spectroscopic measurements and still used to interpret spectroscopic data with unknown pathlengths. However to compensate for anomalies due to scattering in reflectance measurements, refinements have been suggested by, for example, including corrections of the pathlength³¹⁻³⁴, evaluation using mathematical models³⁵⁻³⁸, and compensation for the effective pathlength and optical properties by pathlength resolved³⁹⁻⁴³ or time resolved measurements^{44, 45}.

LIGHT SOURCES

In spectroscopy an essential component of the system is a suitable light source to illuminate the sample, whether it is natural light or an artificial light source. Artificial light sources are usually divided into two broader categories, non-coherent and coherent light sources; where the first can be further divided into five subcategories, filament sources, arc sources, discharge sources, fluorescent sources and light emitting diodes (LED).⁴⁶ The coherent light can be produced by lasers for example, with narrow bandwidth and high energy output. Hence, the light sources possess different properties that give the light certain distinguishable characteristics such as bandwidth, coherence and effective wavelength range.

The selection of light source depends upon the application and the type of spectrometer. Filament light sources with broad spectral characteristic are mainly used in DRS whereas narrowband coherent light sources are used for Raman and fluorescence applications. The chosen wavelength region also affects the energy of the light since the energy of a photon⁴⁷, E [J], is proportional to the wave frequency, ν [s^{-1}], Planck's constant, h [$= 6.626 \times 10^{-34}$ Js] and the speed of light in vacuum, c [$\approx 2.998 \times 10^8$ m/s]. This is defined as⁴⁸:

$$\text{Eq. 7} \quad E = h \cdot \nu = \frac{h \cdot c}{\lambda}.$$

Which yields that the energy of electromagnetic radiation is inversely proportional to the wavelength, i.e. blue light has higher energy than red light. This energy dependence of wavelength for the photons affects the way light can interact with molecules by energy transitions.

OTHER SPECTROSCOPIC TECHNIQUES

In addition to diffuse reflectance spectroscopy a number of different types of spectrometers have been developed for studies of wavelength dependent changes of the light. In the following section some of the most prominent techniques used in biomedical engineering are presented, however the overview is far from complete but covers the most used methods for in vivo diagnostics and tissue characterization in the field of biomedical engineering.

Photon Migration Spectroscopy

Photon migration spectroscopy (PMS), or time resolved spectroscopy, is the study of the migration of photons through matter either in the frequency domain or in the time domain; related to each other by a temporal Fourier transform^{49, 50}. The time domain

utilizes short, Dirac-like, pulses of light and the attenuation and broadening of the pulse is analyzed. In the frequency domain intensity modulated light is used and analysis is based upon changes in the phase and amplitude modulation^{49, 51}.

PMS can be used to characterize and study the optical properties of highly scattering media or perform optical tomography to study tissue volumes. The technique is mainly used in the red and near infrared (NIR) wavelength range and by using multiple wavelengths spectral information can be extracted to estimate thick tissue hemodynamics or perform optical mammography to find malignant tissue.⁴⁹

Raman Spectroscopy

Raman spectroscopy is a method to characterize and study molecules by their, inelastic, Raman scattering. Differentiation of the Raman active molecules is performed by analysis of the resultant Raman shift which acts as the specific “fingerprints”. The method most commonly uses a NIR laser to probe the tissue.⁵²

The Raman method is often used since it is specific and sensitive and it has a small spatial distribution of about a couple of μm^2 . Furthermore, most biomolecules present in human tissue exert Raman scattering and therefore have the potential to be analyzed. However, the drawback is the low occurrence of Raman shifts which can make recordings of the signal cumbersome and time consuming⁵². Raman spectroscopy can be used to discriminate between healthy and pathologic tissue⁵² as well as probing for specific chromophores such as carotene⁵³ and water⁵⁴.

Fluorescence Spectroscopy

Fluorescence spectroscopy, or “luminescence spectroscopy”, is a method where the electronic states of atoms and molecules can be examined by the resulting luminescence after excitation with light. For biomedical applications there are two general methods to characterize tissue, the first uses the inherent, or endogenous, autofluorescence, the second uses exogenous fluorescence. The fluorescence can be analyzed by the emission spectra, quantum yield, lifetime or the polarization.⁴⁹

A frequent use of fluorescence is to differentiate and demarcate pathologic and cancerous tissue from healthy tissue, e.g. atherosclerotic plaque and different kinds of neoplasia. Fluorescence has also been found useful in the treatment of cancer in combination with photodynamic therapy (PDT) where the therapy with photosensitizers can be continuously monitored. The technique can also be used to study cellular structure and metabolism.⁴⁹

ADDITIONAL TECHNIQUES

Spectroscopy is far from the only method that can be used in studies of tissue. Some methods utilize the changes in the spectral signature where others apply different approaches to characterize the tissue. The overview is limited to non-invasive optical technologies and therefore the “golden standard” of histological biopsies⁵⁵ has not been included. Nor has the common method of visual examination been included since that is out of the scope of the thesis focusing on biomedical techniques.

It can be noted that despite the many techniques that have been developed to study the skin, none has proven superior or as Swain and Grant⁵⁶ already concluded about skin blood flow measurements in 1989, “there is not a ‘gold standard’ [...] as different methods sample different parameters.”, a citation that still seems to hold true.

Optical Coherence Tomography

The principle behind optical coherence tomography (OCT) can be found in the Michelson interferometer and the use of low coherent light that is reflected in the tissue; either due to refractive index discontinuities, “tissue reflectors”, or by diffuse backscattering from tissue heterogeneities^{57, 58}. For axial measurement the “echo” time is then registered by an fiber optic interferometer with a reference path giving the time delays and amplitudes of the tissue reflections as a function of the depth^{57, 59}.

The resulting cross-sectional image, tomogram, is built up by performing axial measurement in successive transverse line scans across the area of interest⁵⁹. The recorded signal is usually presented as either false colored or grayscale images⁵⁹ where boundaries between structures can be examined; making it analogue to histological biopsies⁵⁸. Advances in the technique have made it possible to record video sequences and study microcirculatory blood flow⁶⁰. OCT is furthermore on the verge of molecular imaging and the identification of chromophores with techniques using the principle of Raman scattering processes or transient absorption⁶⁰. OCT has been applied in many fields of biomedicine including dermatology⁵⁸ and cardiology⁶⁰, but is used foremost clinically in ophthalmology⁶¹.

Photoplethysmography

Photoplethysmography, PPG, is a low cost optical method that assesses blood volume changes in the vasculature. The PPG-signal is most commonly recorded by transmission measurement but it is also possible to use it in reflective mode⁶². The characteristic signal from a PPG-instrument consists of two components, a pulsatile component superimposed on a relatively constant component which depends on the optical characteristics of the tissue^{56, 63}. The pulsatile signal is normally reported as being caused by rhythmic changes of arterial blood due to the heartbeats. Slower changes in the signal can be attributed to changes in the total blood volume but also by other mechanisms such as breathing and thermoregulation.⁶³

By recording the PPG-signal at two different wavelengths, usually in the red and NIR wavelength range, it is possible to extract information about the oxygen saturation of arterial blood, SaO₂⁶³. This method is known as pulse oximetry and is perhaps the most well known apparatus in daily use in clinical intensive care.

Laser Doppler Flowmetry

Laser Doppler flowmetry, LDF, is a method to characterize the microcirculatory perfusion. The method utilizes monochromatic laser light, usually in the red or NIR wavelength range, and the Doppler shift that occurs when light is quasi-elastically scattered by moving blood cells but also by other tissues in motion. LDF can be realized as laser Doppler monitoring (LDPM) or laser Doppler imaging (LDPI). LDPM, which measures in one point, and is often realized with fiber optics, is suitable for temporal measurements. LDPI systems, which are non-contact systems, can present the perfusion data as pseudo-colored two dimensional images and therefore are suitable for spatial measurements.⁶⁴

Over the years the LDF technique has been used in many diverse applications⁶⁴ including the skin⁶⁵ and the heart⁶⁶.

Microscopic Techniques

The use of microscopy on in vivo tissue is sometimes known as "intravital microscopy" which implies its use to visualize the microcirculation and the state of the tissue⁶⁷. Its usefulness lies in the fact that it is possible to get a visual overview of the tissue and the regional blood flow of the tissue in an instant; while the actual composition of the blood is not analyzed. Modern microscopes are usually hand-held and can capture image sequences which can, for example, visualize the intermittent and sometimes chaotic flow in the capillaries.

Capillary microscopy is a method where a microscope is used to study the distribution and function of capillaries in the skin. It has mostly been used at the nail fold, but it can be applied at any accessible site where it can be used to quantify the capillary distribution as well as study the movement of erythrocytes in the capillaries in either color or grayscale^{68, 69}. Methods have been presented to improve the contrast between the erythrocytes and the surrounding tissue by using polarized light or green light, e.g. orthogonal polarized spectral imaging (OPS)^{67, 70} and sidestream dark field microscopy (SDF)^{71, 72}. Both OPS and SDF produce grayscale images or video sequences where the capillary ultrastructure and the movement of the erythrocytes can be studied.

Confocal microscopy is another technique that can be applied to study different layers of the skin by focusing at one depth at a time. This technique has been used to study structures in the skin as well as pathologic conditions.⁷³

Microscopic techniques have also been applied to differentiate between pathologic tissue and normal tissue in the skin, e.g. cancerous tissue⁷⁴. For this purpose a spectroscopic approach has also been developed⁷⁵.

Camera Techniques

Standard cameras are used during medical practice for documentation and characterization of tissue, and then foremost the skin⁷⁶. To standardize the color of the images can reference standards be used for calibration of the colors in the images⁷⁷. The images can further be standardized with the help of different color spaces such as CIElab^{77, 78} from Commission Internationale de l'Eclairage (CIE).

To characterize certain aspects of the skin, studies have been executed using monochromatic, red and green, light to assess erythema and pigmentation in the skin⁷⁹, as well as using UV-radiation⁸⁰. These methods utilize the variable absorption for different wavelengths and can be a blunt measure but still give an indication of the spatial distribution of the pigmentation¹⁶. To minimize the influence of the surface in the images, techniques utilizing polarized impinging light and orthogonal polarizing filters have been developed^{16, 81}. Recently the use of polarization in combination with separate color bands has been reported as being able to visualize the spatial distribution of blood in the skin⁸².

Erythema Meters

Erythema meters were developed to enable a simple way of studying the degree of reddening of the skin in a small area of the skin (20-

150 mm²), mainly due to inflammatory responses of the skin, e.g. due to UV-radiation. The technique measures the narrowband intensities of green and red light and a ratio denoted erythema index is calculated. This method is based on the fact that an increased blood volume will absorb more green light as compared with red light.⁸³

Different versions have been proposed that can measure in contact with the skin as well as non-contact^{83, 84}. Although it might seem as a crude measure, results have been presented showing good agreement with visual scoring by dermatologists⁸⁴.

Colorimetry

The color of an object is sometimes measured objectively with a colorimeter which measures the object and converts the color to tristimulus values as a numerical representation of human vision. The actual tristimulus values, usually measured by applying three separate filters, are defined by the CIE standard observer. The function of colorimeters has a close resemblance to the function of erythema meters, with the addition that it can also give a measure of the brownness of the skin.⁸⁵

4

*“Describing ‘the’ optics of human skin
is somewhat like describing ‘the’ weather;
it can be measured and understood
but cannot be considered static.”*
Anderson, Parrish, 1982

OPTICAL PROPERTIES

Light illuminating a tissue surface may be reflected, transmitted, or absorbed. The sum of the intensities of these interactions must equal the incident intensity as stated by the conservation law⁵:

$$\mathbf{Eq. 8} \quad I_0(\lambda) = I_{\text{Reflected}}(\lambda) + I_{\text{Transmitted}}(\lambda) + I_{\text{Absorbed}}(\lambda).$$

The refractive index mismatch and the surface structure of the tissue give rise to specular reflection at the boundary between skin and air. The constituents of the volume will then affect the transmission, scattering and absorption of the irradiating light inside the tissue. Despite the specular reflection, the bulk of the incident light will penetrate deeper into the tissue⁸⁶ where it will scatter until eventually absorbed in the tissue or remitted out of the tissue.

The concept of optical properties is a theoretical framework to define the transport of light in the tissue volume by a few parameters. The light interaction with matter is rather complex but the optical properties of a material can be described by a few fundamental components such as the scattering and absorption of the tissue. These properties depend upon the concentration of the tissue constituents as well as the properties of the structures present and how they are arranged. The optical properties also dictate the migration of photons through the tissue that is highly dependent on the wavelength of the interacting light.

The optical properties of tissues are usually defined by the refractive index, n , the absorption coefficient, μ_a [mm^{-1}], the scattering coefficient, μ_s [mm^{-1}], and the anisotropy, g ^{87, 88}.

LIGHT TRANSPORT IN TISSUE

Light transport in tissue is complex due to the intrinsic heterogeneous structure. Nevertheless, it can be described and approximated by simple models and mathematical reasoning using absorption and scattering processes. The absorption is of main interest for analysis of the spectroscopic signal. However, scattering must be considered since it can affect the measured apparent absorption. Besides, if scattering did not occur, the light would propagate in a forward direction until finally absorbed and no remitted light could be recorded. The scattering can also be utilized to derive structural information of a sample.

Light propagation through tissue can be approximated using different mathematical theories and models. The most rigorous approach can be found in the analytical theory, aiming at solving Maxwell's equations, but the mathematical complexity limits its use strongly^{48, 88}.

The transport theory is a heuristic approach which is based on the radiative transfer equation which introduces the absorption coefficient, scattering coefficient, and the phase function. The theory is based on the energy transport through a medium with a homogeneous distribution of scattering particles. However, the difficulty in solving the transport equation exactly limits its use for tissues^{48, 88}.

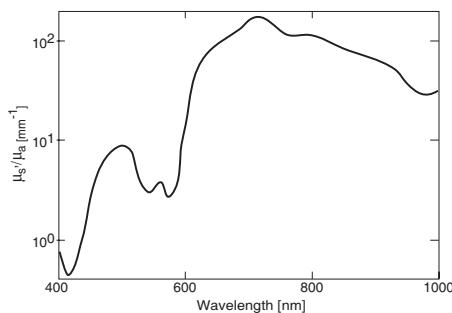


Figure 5: The ratio between absorption, μ_a , and reduced scattering, μ_s' , for skin tissue. (Reproduced and modified with permission from: A. Vogel and V. Venugopalan, "Mechanisms of pulsed laser ablation of biological tissues", *Chemical Reviews*, 103(2), 577-644, 2003. Copyright (2003) American Chemical Society.)

The diffusion theory makes approximations to the transport equation to simplify the calculations. This yields a relatively fast and accurate method handling the diffusion of optical energies along concentration gradients. As the name implies the diffusion theory assumes diffuse light which can be considered valid when scattering predominate absorption, see Figure 5. However, diffusion theory can

be unreliable for small source detector distances and near boundaries of structures with different optical properties^{48, 87, 88}.

The Kubelka-Munk theory, or two flux theory, can be treated as a simplified one dimensional diffusion model discounting reflections at the boundaries. In this model the volume scattering and volume absorption can be determined directly from the reflectance and transmission measurements^{48, 88}.

The Monte Carlo method is a numerical approach using random-walk theory for every photon, basing the results upon the behavior of thousands of photons. Each photon is traced throughout a model of the tissue and checked against probabilities for absorption, scattering, escape, and detection. It is possible to make intricate Monte Carlo models even for small source-detector distances, however, it can be time consuming due to high computational cost^{48, 88, 89}.

Modifications of the Beer-Lambert law have also been proposed, either making assumptions regarding the scattering or by estimating the pathlength the photons have traveled, partly based upon empirical reasoning³¹, but also rigorous theory⁹⁰ and Monte Carlo simulations³⁴.

REFRACTIVE INDEX

The complex representation of the refractive index, $N(\lambda)$, is defined as^{5, 91}:

$$\text{Eq. 9} \quad N(\lambda) = n(\lambda) + ik(\lambda).$$

From which it is possible to derive information about a medium, the real part relating to the scattering effects through the refractive index, n , and the imaginary part relating to the absorption of the tissue since the absorption coefficient relates to the attenuation factor, k , of the complex refractive index by^{91, 92}:

$$\text{Eq. 10} \quad \mu_a(\lambda) = \frac{4 \cdot \pi \cdot k(\lambda)}{\lambda}.$$

The refractive index, n , of homogenous matter describes how the phase speed of electromagnetic radiation in a matter, ν [m/s], changes compared to the speed of electromagnetic radiation in vacuum. This is commonly expressed as:

$$\text{Eq. 11} \quad n = \frac{c}{\nu}.$$

For heterogeneous matter, like tissue, the refractive index can be estimated by volume-weighted average for the different structures⁴⁸.

The values of the refractive index range from ~ 1 in air to higher values in human tissue, for example $1.55_{\lambda=400-700 \text{ nm}}$ for stratum corneum, $1.38_{\lambda=456-1064 \text{ nm}}$ for myocardial tissue, and $1.4_{\lambda=633 \text{ nm}}$ for blood⁹³. It should be noted that the refractive index may display large variations at different wavelengths^{94, 95}.

Using the refractive index it is possible to calculate the angle of refracted light by Snell's law, as well as the amount of light that penetrates the skin by the Fresnel equations⁹⁶. For example the refractive index mismatch of air and the stratum corneum can be shown to account for a about 5% of specular reflection for light incident normal to the skin surface, the remaining 95% will be transmitted and refracted in to the skin before being absorbed or backscattered^{86, 97, 98}. However, the rough structure of the skin may lower this number⁸⁶. The skin-air refractive index mismatch can also cause internal reflection of up to 50% for photons reaching the boundary⁹⁹. Reflection and scattering in the tissue occurs if there is a refractive index inhomogeneity such as between two different tissues, e.g. between blood cells and the surrounding plasma⁹⁴.

ABSORPTION

Absorption is a total transfer of energy from a photon to a molecule, after which the photon cease to exist. A photon, with inherent energy according to Equation 7, can only be absorbed by a molecule if the photon energy corresponds to a difference in energy, ΔE , between two allowed states in the molecules energy levels, E_1 and E_2 . This relationship is defined by Bohr's frequency condition⁵ and correlates to Equation 7:

$$\text{Eq. 12} \quad \Delta E = E_1 - E_2 = h \cdot \nu = \frac{h \cdot c}{\lambda}.$$

The absorption of spectral energy excites the molecule to a higher state and excess energy is lost over time. The loss of energy mostly occurs as heat dissipation, but can also result in the emission of a new photon, perceived as fluorescence or phosphorescence, or as photochemical reactions⁸⁶. The allowable energy levels depend on the molecular structure and vary therefore between different molecules. These energy levels yield that the absorption will vary per wavelength causing the fingerprint by which the molecules can be identified^{5, 48}.

The transfer of photon energy to a molecule can be used to characterize a sample, i.e. spectroscopy, but it can also be used to induce photobiological reactions in the sample, e.g. induction of erythema by UV-radiation^{48, 100} or PDT¹⁰¹.

To describe the absorption of tissue the absorption coefficient is often used, $\mu_a(\lambda)$, as a measure of how long path a photon has to travel in average before being absorbed.

In spectroscopy the chromophores ability to absorb light can be presented as either the absorption coefficient $\mu_a(\lambda)$ [mm^{-1}], the molar absorptivity $\varepsilon(\lambda)$ [$\text{L}/(\text{mol}\cdot\text{mm})$] or the absorptivity $a(\lambda)$ [$\text{L}/(\text{g}\cdot\text{mm})$]^{102, 103}. The former relating to the two others by the concentration of the absorbers as:

$$\text{Eq. 13} \quad \mu_a(\lambda) = \ln(10) \cdot \varepsilon(\lambda) \cdot C = \ln(10) \cdot a(\lambda) \cdot C .$$

Where C is the concentration of the chromophore expressed in mol/L and g/L, respectively. It is crucial to use the correct values if absolute values are sought, otherwise the difference is minute.

SCATTERING

Scattering is either an elastic or inelastic process where the photon experiences a change in direction. Elastic scattering, i.e. without any loss of energy is more frequent than the inelastic Raman scattering, where the photon can both gain and loose energy. Scattering of a photon can even be treated as absorption of the photon followed by the immediate emission of a new photon^{5, 96}.

Scattering is dependent on the size of the scattering particle and the wavelength of the light; based on this assumption the scattering is normally divided into three theoretical ranges. The geometric regime relates to objects much larger than the wavelength of the light. In this regime the direction of the scattered light can be calculated by the difference in refractive index and Snell's law, e.g. for different layers of tissue. The Mie regime relates to objects approximately of the same size as the wavelength of the incident light which translated to tissue conditions corresponds to cellular structures and collagen fibers. Mie-scattering is dependent on wavelength and highly forward directed. The Rayleigh regime is used when the particles are much smaller than the wavelength of the light corresponding to cell membranes and cellular sub compartments. Rayleigh-scattering is almost isotropic and it is inversely proportional to the fourth power of the wavelength. In human skin the dominant scattering is in the Mie-regime and mainly due to the collagen fibers, but all types of scattering can be expected.⁴⁸

In analogy with the absorption coefficient, the scattering coefficient, $\mu_s(\lambda)$ [mm^{-1}], describe how long path a photon has to travel in average before being scattered.

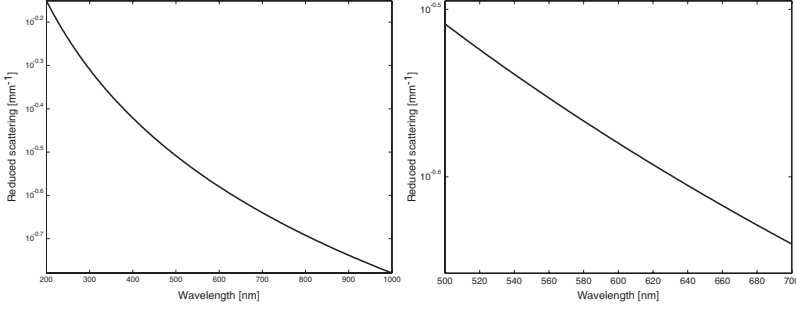


Figure 6: Reduced scattering as approximated by $\alpha\lambda^\beta$. Left panel: scattering in the range 200-1000 nm, right panel, close up of the scattering in the range of 500-700 nm.

Describing scattering as the number of scattering events per distance is not enough, but equally important is the direction of the photon after a scattering event. The distribution of scattering angles can be described by the scattering phasefunction¹⁰⁴, or the anisotropy factor, g , which describes the average of the cosine for the scattering angles, θ , defined as:

$$\text{Eq. 14} \quad g = \langle \cos \theta \rangle$$

The anisotropy factor is often used to describe the overall scattering in the tissue where values close to 0 indicates isotropic scattering, values close to 1 indicates forward scattering, and a value of -1 indicates backward scattering. For tissue the value of g can normally be found in the range of $0.74_{\lambda=476 \text{ nm}}$ to $0.995_{\lambda=665 \text{ nm}}$ ⁸⁸. These values indicate that tissue is mostly forward scattering in its characteristics and it can be presumed that most light remitted from the tissue has been multiply scattered⁵¹.

For diffusely scattering tissue the transport scattering coefficient, or reduced scattering coefficient, $\mu'_s(\lambda)$ [mm^{-1}], is defined as:

$$\text{Eq. 15} \quad \mu'_s(\lambda) = \mu_s(\lambda) \cdot (1 - g)$$

This term has been introduced to reduce the effect of anisotropic scattering and receive a more isotropic scattering for calculations of the photon path³⁹, see Figure 6.

5

*"To him that watches,
everything is revealed."
Italian Proverb*

CHROMOPHORES

The color of skin and other tissues depend on the absorbing and scattering properties of the tissue and foremost it depends upon the distribution ratio and amount of the color-producing pigments present^{6, 81}. These pigments, or chromophores, are the functional groups of the molecules that absorb light in various amounts throughout the spectral band, and hence color the reflected light.

In this thesis, however, the term chromophore is used in the more common wider perspective, i.e. to address light absorbing particles that can be found inherent in the human body. All chromophores have their own characteristic absorption which varies with the wavelength and which can function as a fingerprint for that molecule. Changes in the molecular structure such as binding of other molecules to the functional chromophore will alter the appearance of the absorption and different derivatives of a molecule can thus be found. Cross-over points of two absorption spectra are called isobestic points, i.e. the wavelength where the absorption is invariant to changes in the ratio of two chromophores or derivatives.

The chromophores included in this chapter are limited to those that are endogenous and affect light in the visible wavelength region, but a short overview of chromophores affecting the light in the UV wavelength range can be found at the end of the chapter.

The occurrence and the concentrations of chromophores vary throughout the body and also depend on the type of tissue. The most important and most frequently encountered chromophores are often termed the main or major chromophores of the tissue. Two

chromophores can be differentiated as long as their spectral characteristics differ enough to be separated by the spectrometer. The possibility of examining a chromophore depends on the concentration and the occurrence in the tissue. Chromophores with high extinction coefficients but low concentrations and vice versa are difficult to detect since they will not affect the light sufficiently, which can make them difficult to detect with a spectrometer, e.g. protoporphyrin IX (PpIX) and water respectively.

Data of the absorption coefficients for different chromophores can be found in the literature, however it is rare to find tabulated values for broader wavelength ranges; mostly data is presented for discrete wavelengths. It should be noted that differences in the acquisition of the extinction and absorption coefficients can result in deviations between the tabulated values⁸⁸. A cautious approach is advisable especially if absolute values are sought.

HEMOGLOBIN

Hemoglobin is a large group of hemoproteins responsible for the majority of the oxygen-carrying capacity in the body⁴ and is thus perhaps the most important chromophore for the human being. The chromophore is found in the erythrocytes and is therefore under normal circumstances bound to the lumen of the vasculature network throughout the human body. The actual absorption spectra of the hemoglobin depend primarily upon whether the blood is rich in oxygen or not and correspondingly exists in two main derivatives, see Figure 7.

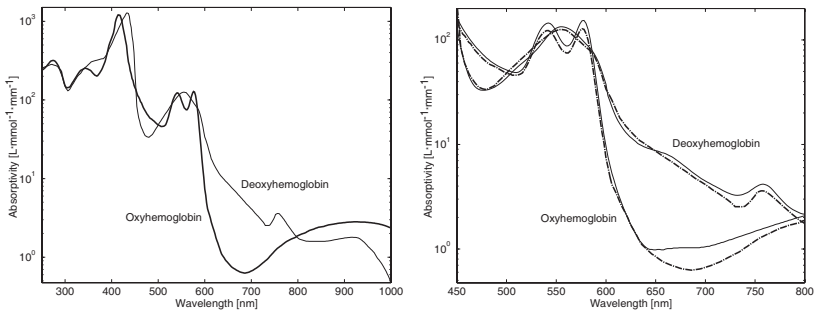


Figure 7: Absorptivity for oxyhemoglobin and deoxyhemoglobin. Left panel: compiled data from Prahl¹⁰⁵. Right panel: comparison between data from Prahl¹⁰⁵, dashed dotted thick line, and Zijlstra et al.¹⁰⁶, thin line; notice the small deviations between the two datasets.

If the hemoglobin has bound oxygen it is termed saturated hemoglobin, or oxyhemoglobin, and the extinction spectra present the characteristic double maxima around 576 and 542 nm as well as

an absorption peak at 415 nm¹⁰³. If no oxygen is bound to the molecule it is termed desaturated hemoglobin, or deoxyhemoglobin where the double peaks of oxyhemoglobin are transformed into a single maxima at 555 nm, as well as there being red-shifting of the peak at 415 to 430 nm. There is also an additional maxima that becomes apparent at 756 nm after reduction not found for oxyhemoglobin¹⁰³. The concentration of hemoglobin for normal adults is approximately 120-180 g/L¹⁴.

Hemoglobin derivatives also exist which do not contribute to the oxygen transport and are therefore collectively known as dyshemoglobins of which methemoglobin and carboxyhemoglobin are reversible but formation of sulfhemoglobin is irreversible^{4, 103}. The dysfunctional derivatives differ in absorption, more or less drastically, compared to the functional hemoglobins, see Figure 8.

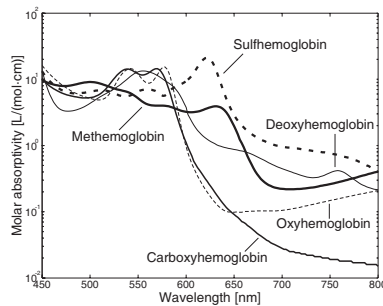


Figure 8: Absorption for all hemoglobin derivatives found in human tissue, data from Zijlstra et al.¹⁰⁶.

Oxidation of the iron in the hemoglobin forms methemoglobin which disables the molecule's ability to bind or release any oxygen. This transformation drastically changes the absorption of the hemoglobin^{4, 103}. The oxidation of hemoglobin occurs continuously in the body but is counterbalanced through a constant reduction⁴. This counterbalancing process reduces the amount of methemoglobin for normal conditions to a maximum of 1% of the total amount of hemoglobin, but congenital methemoglobinemia has been encountered^{4, 14}. The concentration of methemoglobin can increase due to an increased oxidation which can occur, for example, after poisoning or medication⁴. An increased concentration of the methemoglobin can also be found in bruises¹⁰⁷.

The hemoglobin molecule has a high affinity for carbon monoxide and is therefore likely to bind the carbon monoxide molecule⁴. In such cases the absorption of the oxyhemoglobin blue-shifts and compresses slightly and the chromophore is named

carboxyhemoglobin¹⁰³. Normally about 0.5% carboxyhemoglobin can be found in the human erythrocytes partly from endogenous production of carbon monoxide, but this figure increases in environments with high concentration of carbon monoxide; e.g. smoking can result in as high values as 10%⁴.

A third dyshemoglobin is sulfhemoglobin where sulphur has bound to the hemoglobin. This derivative is rare in healthy individuals but is foremost found in individuals that have been exposed to oxidant agents. However, sulfhemoglobin has been found to exist congenitally in a few cases. The binding of sulphur changes the absorption spectra drastically introducing a new prominent absorption maxima around 622 nm.⁴

It can be noted that the occurrence of cyanosis depends on the ratio of the different chromophores. Cyanosis becomes apparent at a concentration of 50 g/L deoxyhemoglobin, 15 g/L methemoglobin or as low concentration as 5 g/L for sulfhemoglobin⁴. Occurrence of carboxyhemoglobin will however not result in cyanosis due to its characteristic absorption closely resembling that of oxyhemoglobin.

MYOGLOBIN

Myoglobin acts as a buffer and diffusion mediator for oxygen in the muscles, but it has also been suggested that it can inactivate nitric oxide and reduce reactive oxygen species. The reddish myoglobin is a hemoprotein just like hemoglobin, but whereas hemoglobin is found in the blood vessels, myoglobin is confined in the striated muscle cells, i.e. the skeletal and heart muscle fibers. The close resemblance in molecular structure of the two hemoproteins makes the absorption similar in appearance to hemoglobin, see Figure 9. The total concentration of myoglobin in the heart has been measured and it is reported to vary from 0.8 in the left atrium to 2.4 mg/g heart wet weight for the left ventricle. Analogous to hemoglobin, myoglobin does normally exist in two derivatives; oxymyoglobin and deoxymyoglobin¹⁰⁸.

Dysmyoglobins such as metmyoglobin, carboxymyoglobin, and ferrymyoglobin do exist, the latter formed as a result of oxidative stress or scavenging of nitric oxide-molecules^{109, 110}. The presence of dysmyoglobins should however be low in normal tissue based on the low occurrence for dyshemoglobins, except for methemoglobin which is constantly formed.

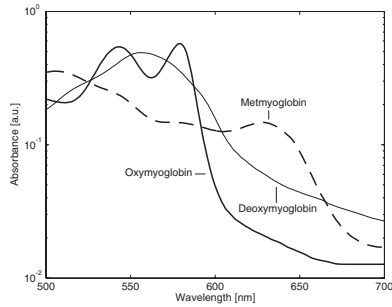


Figure 9: Extinction coefficients for myoglobin derivatives. (Reproduced with permission from: K. A. Schenkman, D. R. Marble, D. H. Burns and E. O. Feigl, "Myoglobin oxygen dissociation by multiwavelength spectroscopy", *Journal of applied physiology*, 82(1), 86-92, 1997. Copyright (1997) The American Physiological Society).

CYTOCHROMES

Cytochromes constitute a wide and disparate group of hemoproteins involved in the electron transfer process. Of special interest is the complex of cytochrome *aa₃*, also known as cytochrome *c* oxidase; which is involved in the last steps of the oxygen transport chain together with cytochrome *b* and *c*¹¹. These cytochromes are located in the inner mitochondrial membrane and the concentration is therefore normally time invariant, but oxidation and reduction changes the perceived absorbance¹¹², see Figure 10.

It can also be noted that the erythrocyte bound cytochrome *b₅*, is involved in the reduction of methemoglobin back to functional hemoglobin⁴.

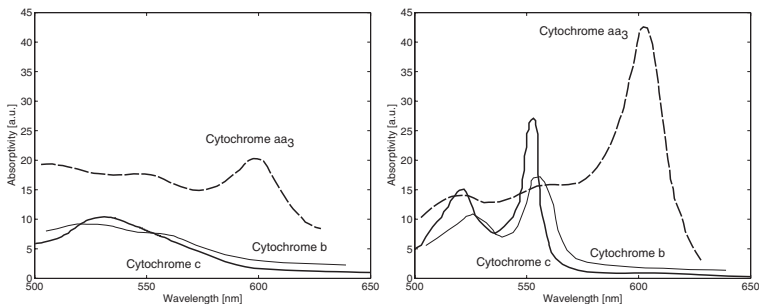


Figure 10: Absorptivity for Cytochromes *aa₃*, *b* and *c*, left panel: oxidized forms; right panel: reduced forms, data from Biomedical Optics Research Laboratory¹¹³, originally presented by U. Henrich¹¹⁴.

BILIRUBIN

Bilirubin is a yellowish residue from the breakdown of hemoglobin foremost in the spleen and liver during the last cycle of the

erythrocytes, see Figure 11. Normally it is absorbed in the liver and secreted into the bile and thus not normally visible in the skin. However it can be seen as jaundice in infants and can also be present in persons with dysfunctional livers, e.g. due to diseases. This is an effect when the liver can not deal with all bilirubin and where the excess assemble in the blood stream and leak out into tissues causing a yellowing of the skin tone.¹³

Bilirubin can also be present in bruised skin due to breakdown processes of extravascular erythrocytes¹⁰⁷. During breakdown of the hemoglobin an intermediate green colored chromophore is formed called biliverdin, this chromophore is, however, short lived^{13, 115}, but may persist in rare cases giving the skin a greenish hue¹⁵.

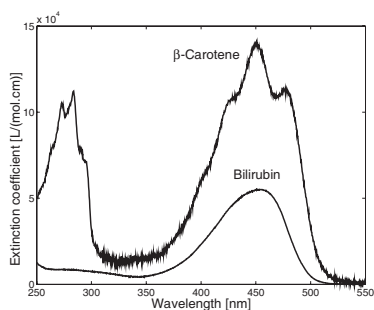


Figure 11: Extinction coefficients for bilirubin and β -carotene, data from PhotochemCAD¹¹⁶ (<http://www.photochemcad.com/>).

MELANIN

Melanin is one of the main chromophores responsible for the coloring of human skin and hair, but also found in the eye. The amount and structure of the aggregated melanin can make the skin go from white to black; as found in Caucasian and Negroid skin. It is also the reason for the facultative change of the skin after exposure to UV-radiation to a darker pigment as a response to the harmful radiation. The melanin is produced in the melanocytes in the stratum basale of the epidermis. From this layer the melanin granules, aggregated in the melanosomes, diffuse out into the keratinocytes of the stratum spinosum via the melanocytic dendrites^{117, 118}.

There are two types of melanin with slightly different absorption spectra, see Figure 12, eumelanin and pheomelanin where eumelanin can be found in Caucasian skin and Negroid skin but pheomelanin is mainly found in Caucasians and in abundance in fair skinned, red-haired individuals^{117, 119}.

It is not the amount of melanin producing units, melanocytes, per square millimeter that determines the color of the skin, but it is rather the size, amount and distribution of the melanosomes in the keratinocytes that differs. Darker individuals have a higher melanin production and wider distribution of the melanin granules even in the stratum corneum. Fair-skinned individuals in contrast have less melanin and the melanin is present as aggregated small melanin granules spread in the epidermis but not present in the stratum corneum.^{117, 118}

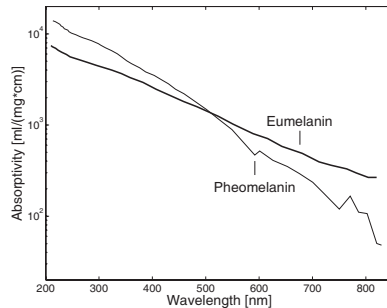


Figure 12: Extinction coefficient for eumelanin and pheomelanin, data provided by Jacques¹²⁰.

The production of melanin in the melanocytes can be affected by chemical or physiological factors as well as a response to actinic injury where the most well known is the UV-radiation from the sun.¹²¹ The onset of melanin production can be immediate or delayed and depends on the dosage and type of UV-radiation¹²².

It has been proposed that melanin extinction is largely due to scattering in the melanin granules. Melanin correspondingly follows a pattern that can be approximated with the function λ^{-4} , hence showing a Rayleigh scattering behavior and the melanin granules can be regarded as scattering particles. The scattering process has been proposed as originating from the structural formation of melanosomes which, to some extent, act as polarizer in the skin.¹²³

CAROTENOIDS

Carotenoids are a collective term for a large group of molecules, of which more than 600 variants exist¹²⁴. The two most common variants are β -carotene and lycopene which can be found in carrots and tomatoes respectively⁵³. Both of these carotenoids may, to some extent act as a sun blocker¹²⁵ when present in the skin since the absorption is most pronounced in the UV and blue wavelength region, see Figure 11. However carotenoids are not only found in the skin but also in the blood stream, aorta and the macula lutea^{6, 126, 127}. To be present in the skin, foremost in the epidermis and

subcutaneous fat, the individual usually has to have a high intake of carotenoid rich food which ultimately will yield a yellowish tint of the skin^{6, 126}. The carotene, with an absorption peak at 482 nm in normal skin spectrum can be found mostly in the facial region, shoulders, palms and soles⁸. The color due to carotenemia could possibly be misinterpreted as jaundice.

LIPIDS

Different lipids, or body fat, can in correlation with water be found throughout the body, e.g. the subcutaneous fat layer and epicardial fat. Adipose tissue containing most of the lipids in different constellations is considered as scattering tissue. However, it can also act as an absorbing substance with its own characteristic absorption¹²⁸, see Figure 13, and in combination with carotenoids it can shift in color to a more orange tint inducing an additional peak of carotene at 455 nm⁸. The concentration of lipids varies for different adipose tissues ranging from 61-87%¹²⁹.

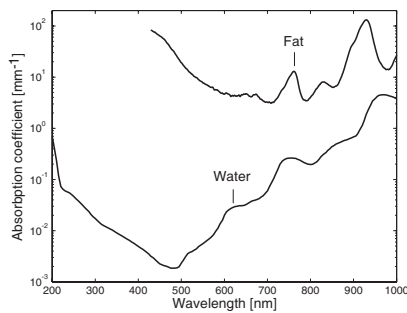


Figure 13: Absorption coefficients for fat, as derived from lard, and water. Data for fat spectra presented by van Veen et. al¹²⁸, data for water spectra presented by Segelstein¹³⁰; data provided by Prahl^{131, 132}.

WATER

Water is a weakly absorbing chromophore in the visible wavelength range but shows increased absorption both in the UV but also in the NIR region, which results in its perceived blue color, see Figure 13. Water is one of few molecules that color light due to pure vibrational states of the molecule¹³³ and it is found throughout the whole body in the intracellular as well as extracellular fluid, e.g. in the plasma of the blood¹⁰. The concentration of water ranges from 11% in adipose tissue to 92% in the plasma in humans¹²⁹.

ADDITIONAL CHROMOPHORES

The total number of endogenous chromophores that can be found in human tissue is vast. However, most chromophores are only present in smaller concentrations, making them less prominent. Others are active in wavelength regions outside of the visible. Some chromophores even emit light after absorption and are hence named fluorophores. A selected few of those minor chromophores are overviewed briefly in this section.

Protoporphyrin IX one of the endogenous fluorophores is a precursor in the hemoglobin synthesis and can be found in very low concentrations in the bloodstream¹³⁴. The absorption for PpIX in the UV and blue wavelength range corresponds to the excitation wavelengths as well as it having a characteristic emission at 635 and 704 nm. PpIX is often used in the characterization of cancer where exogenous PpIX is transformed by ingestion or injection of aminolevulinic acid (ALA), whereafter accumulation occurs in cancerous tissue and this build up can be detected by its fluorescence, but also used for PDT¹³⁵.

The brownish iron pigment hemosiderin is a residue after the macrophages have started decomposition of erythrocytes outside the blood vessels¹³⁶. It occurs due to disease and after hemorrhage and can be found, for example, in the skin⁸¹ and the heart¹³⁷. It is of interest since it has been suggested that the presence of hemosiderin can be an indicator of pathologic conditions such as stasis dermatitis, lipodermatosclerosis and even ulceration¹³⁶.

DNA and urocanic acid can be found in the skin and both acts as filters for UV-radiation. These chromophores absorb mainly in the UV wavelength region and have almost no absorption in the visible wavelength region. Other chromophores present in the UV-range include proteins and vitamins such as tryptophan, tyrosine, and riboflavin. The co-enzymes NADH and NADPH involved in vascular regulation and reduction of methemoglobin, can also be found in the skin.¹³⁸

6

*"The wise man says,
'I am looking for the truth,'
and the fool says,
'I have found the truth'."*
Russian proverb

AIMS OF THE THESIS

The general aim of this thesis was to develop and evaluate diffuse reflectance spectroscopy (DRS) techniques for assessing tissue chromophores related to tissue oxygenation and pigmentation. Specifically, the aims were:

- To propose decomposition algorithms for estimating the concentration of tissue chromophores using DRS recordings from skin tissue and heart muscle.
- To evaluate in vivo changes of chromophore content in experimental and clinical settings.
- To investigate the spatial distribution and heterogeneity of the chromophore content in stimulated skin.
- To develop and demonstrate a DRS hyperspectral imaging system for spatial and temporal assessment of tissue chromophore concentrations in superficial tissue.

7

*"I have always considered myself
more an explorer than a scientist..."*
Frans F. Jöbbsis-vanderVliet

SPECTROSCOPY AS APPLIED IN THE THESIS

This thesis considers spectroscopic measurements in the visible wavelength range, covering two different types of tissue, heart and skin, and the characterization of changes in the microcirculation. Measurements have been made in such different settings as the operating theater and the more controlled environment of a laboratory using provocations, i.e. heat and UV-radiation. The analysis of recorded spectra can be carried out using complex models and theories, analytical or numerical analysis, or straightforward methods using the Beer-Lambert law and modifications thereof. Depending on the situation, different solutions should be considered using the most appropriate methods and models. If exact values of the chromophore concentrations are of interest then it is necessary to apply advanced techniques and analysis. If changes or relative values are sufficient, simplifications and approximations can be made, as long as the requirements are met for the specific situation.

The thesis constitutes straightforward analysis, prioritizing speed and observational spectroscopy, Paper I, II and IV, but does also include measurements yielding absolute values, Paper III. To compare the assumed model spectra with measured spectra, linear and nonlinear, curve fitting in a least-square sense has been used to employ as much of the spectral data as possible and in an effort to make the analysis more robust against noise.

PREPROCESSING OF SPECTRA

Before spectral analysis of recorded reflectance spectra can begin, some simple preprocessing has to be executed. As a first step it is recommended that a visual inspection of the recorded data is performed to identify any outlier in the recordings that may disturb later analysis. If outliers are found, potential explanations for the erroneous result needs to be identified before the data can be removed. It is important to have strict criteria for removal to ensure that data are not removed unnecessarily or even gratuitously.

To increase the SNR of the recorded spectra, as well as to compensate for small temporal fluctuations of the signal, a time average can be calculated from the recorded spectra. An alternative strategy for increased SNR is the use of filtering of the spectral signal over the wavelength band.

The next step of the preprocessing is the normalization, or compensation, of the system parameters and the intensity profile of the light source. This is normally done by measuring the reflectance of the incident light using a white reference standard; in this thesis reference standards included PTFE-tiles and custom made intensity references. Normalization is then carried out by calculating reflectance or absorbance according to Equations 1 or 2 respectively. Based on early experiences in Paper I it was found that it is useful to continuously record the light intensity of the light source to keep track of unexpected fluctuations in the light source intensity. This can, in practice, be realized by using bifurcated fibers, or separate fibers, leading light from the light source, directly or by a standard reference, to a separate channel of the spectrometer.

However, the channels of a spectrometer are usually realized as separate spectrometers using different optical components and detectors, thus making it necessary to correlate the two channels against each other. Different optical benches will also cause the wavelength per detector element to differ. Hence, the channels must be normalized against each other and any wavelength discrepancy must be corrected. Calibration light sources, with well defined emission peaks, can be used to examine any discrepancy between channels. Wavelength discrepancies can be compensated for by software and mathematical interpolations. Normalization can be performed by making simultaneous measurements of the two channels, M_{Master} and M_{Slave} , using a white reference standard and correcting the average of the measurements by the difference thereof as follows:

$$\text{Eq. 16 } M_{Master,Corrected}(\lambda) = \frac{M_{Master,Tissue}(\lambda)}{M_{Slave,LS}(\lambda)} \cdot \frac{I}{\frac{M_{Master,Whiteref}(\lambda)}{M_{Slave,LS}(\lambda)}}$$

The different indices correspond to the continuous measurements of the light source, *LS*, and a single initial measurement of a white reference standard, *Whiteref*. This relation should be checked periodically to ensure that no change has occurred over time. It should at the very least be performed whenever the spectrometer has been moved or its components have been disassembled, but ideally before and after every measurement session to ensure that the correct spectrum is used for normalization.

It is not always feasible, or practical, to record reference measurement of a white standard reference in connection to a measurement session. Further, it can even be more convenient to use a custom-made intensity reference that suits the probe, and simplifies the reference measurements, to keep track of intensity variations between sessions. Then it is possible to correct the measurements, for intensity variations and discrepancies between detectors, by making an extensive reference measurement at a separate occasion, by:

$$\text{Eq. 17 } M_{Master,Norm}(\lambda) = \frac{M_{Master,tissue}(\lambda)}{M_{Slave,LS}(\lambda)} \cdot \frac{I}{\frac{M_{Master,Intref}(\lambda)}{M_{Slave,LS,Intref}(\lambda)}} \cdot \frac{\frac{M'_{Master,Intref}(\lambda)}{M'_{Slave,LS,Intref}(\lambda)}}{\frac{M'_{Master,Whiteref}(\lambda)}{M'_{Slave,LS,Whiteref}(\lambda)}}$$

Where *M* denotes measurements carried out at each measurement session and *M'* denotes measurements made at a separate occasion in time. The indices correspond to measurements of the tissue, *Tissue*, and intensity reference respectively, *Intref*.

DIFFERENCE SPECTRA

Situations often occur when measurements are made on different occasions, or at different sites, where the only interest is any change in chromophore content during the measurements, spatially or temporally. Under these circumstances it may be useful to calculate the difference spectra of the two measurements in an effort to remove the background signal from the observations.

Consider two different measurements recorded on two separate occasions with the same setup. They can then be assumed to yield two different absorbances, A_1 and A_2 , with corresponding incident

intensities, I_{01} , I_{02} , it is then possible to calculate a difference spectrum, $A_{Difference}=A_1-A_2$, as:

$$\text{Eq. 18} \quad A_{Difference}(\lambda) = \log\left(\frac{I_{01}(\lambda)}{I_1(\lambda)}\right) - \log\left(\frac{I_{02}(\lambda)}{I_2(\lambda)}\right) = \log\left(\frac{I_{01}(\lambda) \cdot I_2(\lambda)}{I_1(\lambda) \cdot I_{02}(\lambda)}\right).$$

If, in addition, the incident intensity, I_0 , for the two measurements, can be assumed to be time invariant and equal, then it is possible to further simplify the equation:

$$\text{Eq. 19} \quad A_{Difference}(\lambda) = \log\left(\frac{I_2(\lambda)}{I_1(\lambda)}\right) = \log\left(\frac{I_0(\lambda) \cdot e^{-\varepsilon_2(\lambda)l_2}}{I_0(\lambda) \cdot e^{-\varepsilon_1(\lambda)l_1}}\right) = \varepsilon_2(\lambda) \cdot l_2 - \varepsilon_1(\lambda) \cdot l_1.$$

Hence, by using Equation Eq. 19 it is possible to estimate the relative changes in the chromophore content between the two measurements, by using one measurement as a reference, without the need for separate normalization by measurements of a white reference standard. The final approximation that is made is that the average pathlength for the two measurements l_1 and l_2 is equal yielding the apparent difference absorbance:

$$\text{Eq. 20} \quad A_{Difference}(\lambda) = \varepsilon_2(\lambda) \cdot l_2 - \varepsilon_1(\lambda) \cdot l_1 = (\varepsilon_2(\lambda) - \varepsilon_1(\lambda)) \cdot l.$$

Although rough approximations are necessary, a cautious use of Equation 20 makes it possible to study changes in chromophore content diminishing any absorbance in the bulk tissue as well as influence from scattering, assuming a relatively constant pathlength. However, in reality it is always useful to perform reference measurements to ensure stable conditions.

SPECTROSCOPIC MODELS

To analyze the chromophore content of tissue it is possible to make a first rough approximation that Beer-Lambert law is valid for the spatial and temporal difference spectra of tissue. This approximation will then be based on a constant scattering and bulk absorption of the tissue over time and space, or that any discrepancies thereof can be neglected. The pathlength, l , must also be approximated and preferably be set to be constant to fulfill the second assumption for using the Beer-Lambert law. These rough approximations can give plausible relative data, but usually it will result in low values for the goodness of fit¹³⁹ indicating a bad approximation. Still it can be used to identify the presence of chromophores. The absorbance can then be expressed as:

$$\text{Eq. 21} \quad A_{Difference}(\lambda) = \Delta\mu_a(\lambda) \cdot l = \sum_i \Delta C_i \cdot \mu_{a_i}(\lambda) \cdot l$$

where $\Delta\mu_a$ is the change in absorption coefficient, ΔC_i is the change in concentration for chromophore i and μ_{ai} is the absorption coefficient for chromophore i . Scattering affect the light propagation in the tissue and should therefore be introduced into the analysis to some extent. In fact, to be able to study something other than relative values of the chromophores, more interest must be paid to the scattering processes in the tissue. Scattering will, in general, increase the pathlength for the photons that reach the receiving fiber compared to the actual physical distance. The change in pathlength will vary with wavelength due to the wavelength dependence of scattering.

Combining the change in photon pathlength and the scatter dependent attenuation of the intensity, and using empirical reasoning³¹, or extensive calculus^{90, 140, 141}, a relation between absorbance and scattering can be formulated. This was originally proposed for time-resolved transmission¹⁴², as¹⁴³:

$$\text{Eq. 22} \quad A(\lambda) = \mu_a(\lambda) \cdot DP + G,$$

or¹⁴¹:

$$\text{Eq. 23} \quad A(\lambda) = \mu_a(\lambda) \cdot \overline{\langle L \rangle} + G,$$

where G is a term that only depends on μ_s and the phase function, representing the scattering losses in the tissue not accounted for by absorption. Further, DP is the differential pathlength that depends on μ_a , μ_s , the phase function and the actual geometry, or alternatively is L the (mean) pathlength, both are used under the assumption that neither DP nor L depend on μ_a .^{141, 143}

The true value of G is usually not possible to derive from a single measurement. Nevertheless, by calculating the difference spectra of two measurements, it is possible to derive absolute values for the changes over time in a tissue, as long as the differential pathlength factor can be approximated, since the scattering term of G is cancelled out by this procedure.³¹

Making these approximations and forming a difference spectrum can lead to a modification of the Beer-Lambert relationship with multiple chromophores by introducing a wavelength dependent pathlength, the geometrical pathlength, $l(\lambda)$, as follows¹³⁹:

$$\text{Eq. 24} \quad A_{\text{Difference}}(\lambda) = \Delta\mu_a(\lambda) \cdot l(\lambda) = \sum_i \Delta C_i \cdot \mu_{ai}(\lambda) \cdot l(\lambda).$$

This is an approximation which has been shown to be applicable for reflectance measurements while accounting for some of the

attenuation from scattering¹³⁹. Equation 24 is however only applicable for small changes in the chromophore concentration since large changes in the absorption may introduce non-linear effects. Still it is useful to give rough estimates of the concentrations of chromophores¹⁴⁴.

It has also been verified by Monte Carlo simulations, that for small fiber separations and by analyzing DRS spectra over shorter wavelength bands, Equation Eq. 22 can be approximated by³⁴:

$$\text{Eq. 25} \quad A(\lambda) = \mu_a(\lambda) + \delta + \gamma \cdot \lambda.$$

where the scattering dependent factor G is approximated by introducing a wavelength dependence by the variables of δ and γ . The approximations are suggested to be useful for studies of pigmentation and erythema despite the rough handling of the scattering³⁴.

Another empirical more refined approach, where non-linear scattering effects have been taken into account, has been proposed by Jacques et al.¹⁴⁵. This includes a calibration procedure of the measurement probe against known optical properties. The analogous expression for the transport of light in the tissue from emitting to receiving fiber is defined as^{42, 145}:

$$\text{Eq. 26} \quad T(\mu'_s, \mu_a) = \frac{M_{\text{Tissue}}}{M_{\text{Whiteref}}} = K \cdot e^{-(\mu_a \cdot L)},$$

where K correspond to the attenuation of the scattering as approximated by:

$$\text{Eq. 27} \quad K = a + b \cdot \mu'_s + c \cdot \mu'^2_s,$$

and L corresponds to the change in pathlength due to scattering as approximated by:

$$\text{Eq. 28} \quad L = d + e \cdot \mu'_s + f \cdot \mu'^2_s.$$

The calibration factors, a to f , in Equation 27 and 28 depend on the geometry of the measurement probe and the measurement setup¹⁴⁶. Hence, for a given setup, these factors can be determined using calibration measurements from a set of phantoms with known optical properties, preferably spanning the possible values found in tissue.

The reduced scattering coefficient in Equation 26 and 27 is modeled by an approximate expression⁴²:

$$\text{Eq. 29} \quad \mu'_s(\lambda) = \alpha \cdot \left(\frac{\lambda}{700} \right)^{-\beta}$$

that closely resemble the MIE scattering of tissue¹⁴⁷, where α and β are free model parameters. The absorption is modeled as the linear combination of the chromophores that are found in tissue. For the heart, the absorption can be modeled as:

$$\text{Eq. 30} \quad \mu_a(\lambda) = f_{Hb+Mb} \cdot (S \cdot \mu_{aHbO_2}(\lambda) + (I-S) \cdot \mu_{aHb}(\lambda)) + f_{Water} \cdot \mu_{aH_2O}(\lambda) + f_{Lipid} \cdot \mu_{aLipid}(\lambda).$$

where f is the fraction of the chromophores and S the tissue oxygenation. Both f and S are free model parameters while the chromophore absorption coefficients μ_{aX} are known in advance. Note that the fraction of hemoglobin and myoglobin, f_{Hb+Mb} , were not separated in Paper III but represented by hemoglobin since Hb and Mb are almost indistinguishable. The respective absorption coefficient indices correspond to: HbO_2 , oxyhemoglobin; Hb , deoxyhemoglobin; H_2O , water and $Lipid$, fat.

CURVE FITTING

In order to decompose the spectral content of recorded absorbance data, linear or non-linear regression can be used when a model of the absorbance is fitted against the measurements. The model can be complex or approximative and a priori knowledge of the tissue is favorably used to form the model. For a simple Beer-Lambert model, linear regression can be used when fitting the absorbance:

$$\text{Eq. 31} \quad A_{Model}(\lambda) = \mu_a \cdot l = (p_1 \cdot \mu_{a1}(\lambda) + p_1 \cdot \mu_{a2}(\lambda) + \dots + p_n \cdot \mu_{an}(\lambda)) \cdot l$$

to measured spectra. The unknown factors, p_i , of the known chromophores $\mu_{ai}(\lambda)$, in the model indicate the fractions of each chromophore that possibly can account for the total measured absorbance, $A(\lambda)$.

The actual estimates for the unknown factors, p_i , are found by minimizing the sum of squares, F , of the recorded absorbance $A(\lambda)$ and the model, $A_{Model}(\lambda)$ in a least square sense by¹⁴⁸:

$$\text{Eq. 32} \quad F = \sum (A(\lambda) - A_{Model}(\lambda))^2 = \|A(\lambda) - A_{Model}(\lambda)\|_2^2.$$

The nature of spectroscopic data makes it convenient to use the matrix notation¹⁴⁹ for the equality of measured spectra \mathbf{A} and the linear model \mathbf{A}_{Model} , yielding:

$$\text{Eq. 33} \quad \mathbf{A} = \mu_a \mathbf{P}.$$

Equation 32 can then be solved using the normal equations as¹⁴⁹:

$$\text{Eq. 34 } \mathbf{P}_{\text{Estimate}} = (\boldsymbol{\mu}_a^t \boldsymbol{\mu}_a)^{-1} \boldsymbol{\mu}_a^t \mathbf{A}.$$

where $\mathbf{P}_{\text{Estimate}}$ is a vector containing the estimates for p_i as elements and \mathbf{t} is the matrix transpose. For nonlinear models, e.g. Equation 26, iterative approaches must be used, such as maximum-neighborhood algorithms, e.g. the Levenberg-Marquardt algorithm¹⁴⁸.

During curve fitting of spectroscopic signals it is customary to put non-negativity constraints on the chromophores included in the model due to the physiological nature of the measurements. However, when considering difference spectra, negative factors can be found for chromophores if a decrease has occurred from one measurement to another.

ASSESSING THE CURVE FIT

Assuming a valid model, the goodness of fit between the model and the measured spectra can be estimated by different methods, the first being the trivial visual inspection of the two spectra. Visual inspection can be of importance when identifying any outliers, but, to objectify the results of a model, mathematical equations from statistics can be used.

The residual, which is the measure of the fitting error between the spectra and the model is defined as¹⁴⁹:

$$\text{Eq. 35 } \rho_{\text{Error}}(\lambda) = A_{\text{Model}}(\lambda) - A(\lambda).$$

The residual values should be as low as possible to indicate a good fit, and this is achieved by means of the actual curve fitting. It should be noted that the residuals are not scale invariant, so caution is advised when comparing two separate methods of analysis. Studying the residuals can be rather informative for spectroscopy, since they can be used to find any hidden chromophores not included in the model. This is done by examining the residuals for any systematic characteristics in the spectral distribution that might explain a poor fit, and that resembles any known chromophore. The found chromophore can then be included in the model and a new iteration of curve fitting can be performed, hopefully decreasing the residual values. One approach, to minimize the influence of the nature of data, is to normalize the residuals by the measured spectra, which yields percent values for the residual error⁴².

For a more objective measure, it is better still to use the square root of Pearson product-moment, R^2 . This measure is independent of origin and scale and calculates the relationship between a model and the measurement by¹⁴¹:

$$\text{Eq. 36} \quad R^2 = \frac{\left(\sum A(\lambda) \cdot A_{Model}(\lambda) - N \cdot \overline{A(\lambda)} \cdot \overline{A_{Model}(\lambda)} \right)}{\left(\sum A^2(\lambda) - N \cdot \overline{A^2(\lambda)} \right) \cdot \left(\sum A_{Model}^2(\lambda) - N \cdot \overline{A_{Model}^2(\lambda)} \right)}$$

where, \overline{A} and $\overline{A_{Model}}$, are the mean values of the measurement and the model respectively; N correspond to the number of samples in the used wavelength band. The value of R^2 is then used as a quality measure of how well the model resembles the measured spectra; a value close to 1 can be interpreted as a perfect match but a number close to 0 means that there is no linear correlation between the two at all^{149, 150}. Which values for R^2 are to be considered as good depends on the application and nature of the data.

8

“Imaging spectroscopy tells us what is where.”
Bearman, Levenson, 2003

HYPERSPECTRAL IMAGING

This chapter describes the development of a spectral imaging system and its evaluation by measurements of spatial distribution and temporal variations of chromophores in the skin. Findings not achieved by point measurements, or by scanning procedure were achievable with the DRS imaging technique, utilizing simple algorithms. Hyperspectral imaging (HSI), or simply spectral imaging is not a special technique per se, but rather, the combination of techniques for producing spectroscopic images; i.e. a spectrum for each pixel in an image.

GENERAL ASPECTS

The formation of spectral images has its origin in remote sensing where, for example geologic information is retrieved over large geographical areas. However, with the development of the individual components in HSI-systems, the method has also been introduced into the field of biomedical applications, e.g. to detect the spatial distribution of melanin, water and hemoglobin in the skin¹⁵¹,¹⁵², discrimination between oxyhemoglobin and deoxyhemoglobin in the heart¹⁵³, for the characterization of wounds¹⁵⁴ and bruises after trauma¹⁵⁵ and for investigating cancerous tissue by fluorescence imaging¹⁵⁶.

The spectral images are acquired, either by recording an intensity image for each wavelength, or, by recording a spectrum in every spatial point and assigning it to the corresponding pixel; a converse approach is to illuminate the sample with monochromatic light and

thereby resolving the spectral content. Specifically the spectral acquisition can be realized through a variety of different techniques, including liquid crystal tunable filters (LCTF), acousto-optic tunable filters (AOTF) and two-dimensional holographic gratings. Whatever approach is chosen, the result is a hyperspectral data set, or hypercube, comprising both spatial and spectral information. The resulting hyperspectral data sets, which tend to be quite large (image size×bits per pixel×the number of spectral bands), are analyzed for their spectral content as well as for the spatial distribution of chromophores in the image.¹⁵⁷

The obvious advantage of hyperspectral imaging, compared to ordinary single-point spectroscopy, is the addition of high resolution spatial information of the tissue under study. Thereby the spatial distribution of the spectrally decomposed data can be evaluated using classical image processing methods. This is useful since it can generate an assessment of tissue viability in an area, for example delineation of a region of interest (ROI), and spatial, or morphological measures of a skin UV reaction. The imaging system also provides a large number of spectra for the whole field of view (FOV) in a relatively short amount of time compared with recording the same number of spectra point-by-point. Disadvantages may however be coarse spectral resolution and a rather long acquisition time to cover a complete wavelength range. Nevertheless, since HSI is a non-touch technique, sterile conditions are maintained which is necessary in many clinical applications, e.g. the assessment of ulcerating lesions. Additionally, artifactual changes caused by the pressure of a probe can be avoided.

THE HARDWARE

A spectral imaging system was developed for chromophore assessment of the microcirculation comprising a spectral filtering approach using commercially available components. The system was realized with a computer controllable LCTF of type, VariSpec™ (Cambridge Research & Instrumentation Incorporated, USA). Based on previous research, a wavelength range covering most of the visible light from 400 to 720 nm was chosen.

The detector of the system consists of a computer controllable monochromatic camera (Dolphin F-145B, Allied Vision Technologies GmbH, Germany) with a firewire interface enabling fast data transfer of up to 15 frames per second. The sensor of the camera is a charge-coupled device (CCD) with favorable characteristics in the chosen wavelength region, see Figure 14, and with a dynamic range of 12 bits, i.e. 4096 levels. What is more important is that the camera has a

variable sampling time and the possibility of binning the pixels. Both of the features added flexibility to the configuration of the camera and enabled adjustments to match the variations of light intensities encountered. It was found that binning of two pixels vertically and horizontally resulted in good sensitivity and dynamics for measurements on the skin while still maintaining a resolution of 520×696 pixels.

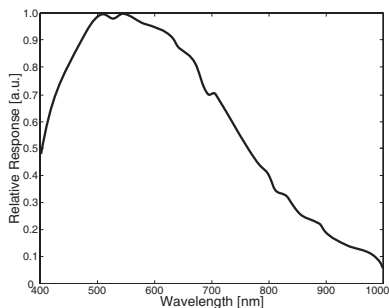


Figure 14: Detector sensitivity of the camera in the hyperspectral imaging system, data normalized to peak.

The collecting optics constituted a normal camera lens (Zoom 7000, Navitar Inc., USA) which enabled focusing of the image plane as well as six times magnification enabling close-ups of the skin.

The “disperser” of the system, realized by the LCTF, was placed in front of the lens enabling imaging of separate image planes for each wavelength. The front-of-lens configuration for the LCTF and optics was chosen for ease of implementation with a single lens, despite possible vignetting effects that can be encountered with this setup. The vignetting effects could be diminished by limiting the used FOV, still covering an area of 38×29 mm.

The light source (ILP ACIS-100/100, Volpi AG, Switzerland), consists of 384 white LEDs arranged in a matrix behind an opaque diffuser. The tissue is illuminated uniformly through a semi-transparent mirror, which resides in the optical path of the system. The light source was chosen because of its uniform, and acclaimed, diffuse light but foremost for its favorable spectral characteristics with high radiance where hemoglobin absorbance is prominent, see Figure 15.

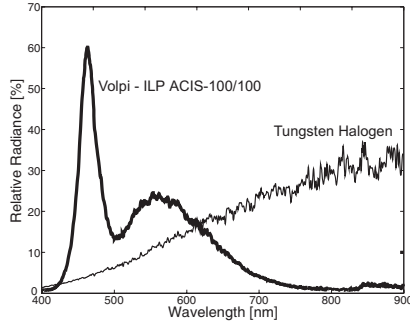


Figure 15: Relative radiance of the light source used in the hyperspectral imaging system compared to a standard tungsten-halogen, filament, light source.

The spatial resolution of the system was limited by the system's optical zoom (6× magnification), the CCD array, and individual sensor elements size (1040×1390 elements with a size of 6.45×6.45 μm) while the spectral resolution is described as the full width at half maximum (FWHM) of the LCTF (10 nm). The total recording time of a hypercube varied depending on the integration time and the number of wavelength bands, but was approximately 40 seconds at the most.

NORMALIZATION

Elimination of the influence of the system parameters and intensity normalization can be performed in two ways for an image system. A reflective standard can be included in the FOV of the system, or using a technique analogous to that used for DRS, i.e. recording reference images before and after any recording. The chosen method was to record reference images before and after a measurement session in order to view as much of the scene as possible, and to be able to compensate for the vignetting effects of the lens setup. A standard white reference, being a color chart (Gretag Macbeth®, Color Checker®, Munsell Color Services, USA) that covered the complete FOV was used to record reference images; BaSO₄ was used occasionally in the beginning, but the color chart proved to be sufficient and more practical to use during measurements and no difference could be detected. The normalization effectively took away any remaining vignetting effects, creating uniform images. The procedure was defined by the calculation of the apparent absorbance for each pixel, i, j , in the image as:

$$\text{Eq. 37} \quad A_{i,j} = -\log \left(\frac{S_{i,j}}{S_{0,i,j}} \right)$$

where $S_{i,j}$ is the intensity signal from pixel i,j from a tissue image and $S_{0_{i,j}}$ correspond to intensity signal from a reference measurement.

SOFTWARE AND ANALYSIS

A graphical user interface was implemented in Matlab (Mathworks Incorporated, USA) to both visualize the images during recordings and to control the detector and LCTF synchronously. Separate software for the analysis of the hypercubes was also implemented in Matlab.

The recorded hyperspectral cubes were analyzed pixel by pixel for the spectral content, which yielded more than 350000 spectra to analyze per image acquired, in less than one minute, prompting for a time efficient analyzing method. It was resorted to curve fitting with non-negativity constraints and a slightly modified Beer-Lambert model, proposed by others^{158, 159}. The chromophores included in the model were oxyhemoglobin, OH , deoxyhemoglobin, DOH , melanin, $Melanin$, and an offset, O , accounting for differences in the intensity and possibly some scattering effects in accordance to Equation 23. For each pixel position, i,j , the absorbance was hence modeled as:

$$\text{Eq. 38 } A_{\text{Model},j} = p_{OH,j} \cdot \mu_{aOH,j}(\lambda) + p_{DOH,j} \cdot \mu_{aDOH,j}(\lambda) + p_{Melanin,j} \cdot \mu_{aMelanin,j}(\lambda) + p_{O,j} \cdot O_{i,j}.$$

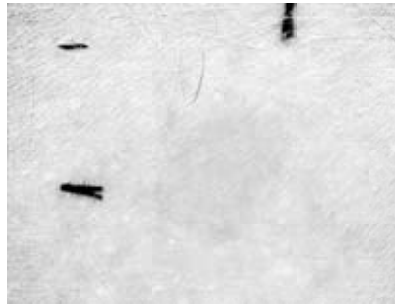


Figure 16: Artificial image of the R^2 -values for the decomposition algorithm, bright parts represent good fit and dark spots represent bad fit, the latter corresponding to black pen marks on the skin in this case.

Using the relative factors received from the spectral decomposition, images could be produced for each of the three chromophores, revealing the spatial heterogeneity of each chromophore. An additional image was produced displaying the calculated R^2 -values, enabling an overview of the goodness of fit for the complete FOV, see Figure 16. This was done foremost to examine if any spatial differences in the curve fitting were present. Before being displayed, all images were filtered with a median filter (7×7 kernel) to reduce

spatial noise, and to enhance the perceived image quality. However, data processing was performed on original unfiltered data. Eventually the spatial information of the chromophores was used to examine the spatial distribution of the chromophores.

EVALUATION OF THE SYSTEM

To evaluate the functionality of the hyperspectral imaging system, initial measurements of pure hemoglobin were chosen. Foremost as a test of the functionality of the system, but also to test if standard values for hemoglobin extinction coefficients could be derived for later use. This was realized by measuring through a specially designed cuvette filled with hemolyzed blood.

Before the measurements, the sample had to be prepared by hemolyzing freshly drawn and heparinized blood and by separating the hemoglobin and plasma with a centrifuge. Changes in the oxygenation were achieved with a tonometer using oxygen and nitrogen, for oxygenation and deoxygenation respectively.

Oxygenation of hemoglobin, however, occurs spontaneously through the pure oxygen pressure of air, which makes it difficult to achieve full deoxygenization of the hemoglobin. To circumvent this, a procedure where all containers in contact with deoxygenized hemoglobin were kept in a nitrogenous surrounding prior to the measurements was implemented, and as a reference of achieved deoxygenation a biochemical laboratory was used. Using this protocol it was possible to achieve absorption curves corresponding to those found in the literature, see Figure 17. It was also possible to study the gradual transformation of deoxygenation into oxygenized hemoglobin.

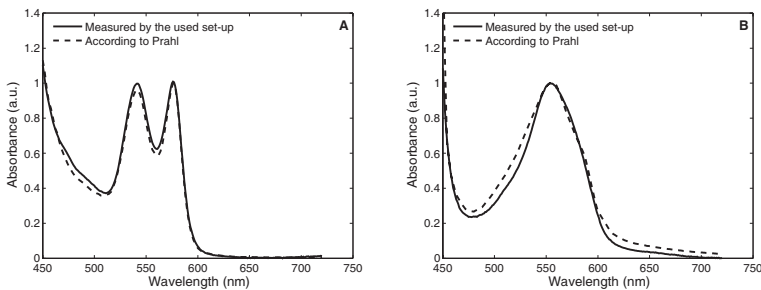


Figure 17: Acquired oxyhemoglobin, A, and deoxyhemoglobin spectra, B, in comparison with tabulated values from Prahl¹⁰⁵ (<http://omlc.org.edu/spectra/hemoglobin/summary.html>).

Additional tests were carried out *in vivo* to study both the possibility to decompose recorded spectra into separate chromophores and also to display the spatial extent of the analyzed chromophores. This was

performed using localized UVB-irradiation, which should induce erythema and possibly also induce an increase of the local melanin concentrations. The erythematous response should be identifiable in the oxyhemoglobin images as a response that increases rapidly during the first hours after provocation. The actual geometry of the provocation should also be quantifiable using graded provocations and sharp edges correspondingly. The extent and the degree of UV-induced erythema is highly dependent on the subjects skin type as classified by Fitzpatrick's classification system¹²². Therefore three subjects covering skin type I to III were included in the study to ensure various responses. Skin type I and II were expected to have a stronger erythema response than skin type III. Furthermore, skin type III could possibly present an increase of the melanin content. Measurements of the responses covered the first 24 hours for assessment of the erythema response and up to 336 hours for the melanin assessment to ensure enough time for an increased melanin production to be detected, see Figure 18.

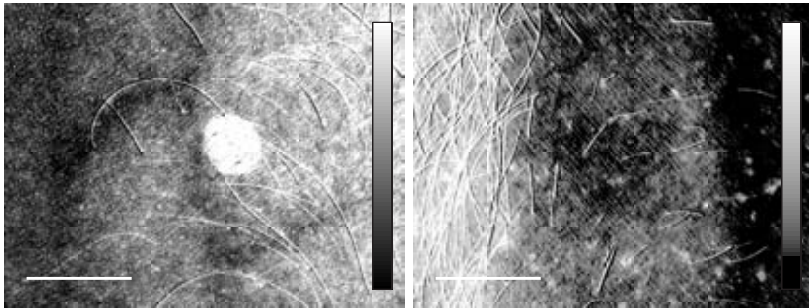


Figure 18: Examples of melanin images based on the factors from the decomposition algorithm, white areas correspond to high melanin factors. The white spot in the left image corresponds to the site of the UVB provocation. Smaller, bright spots found in the right image correspond to freckles.

One set of data was recorded with 1 nm intervals, while the rest were recorded by steps of 5 nm. This was carried out to test if there would be any differences between the different modes of recording. With this setup for evaluation it was expected that the sensitivity of the system to different responses as well as the extraction of spatial information could be tested in a few measurements.

9

*"A theory is something nobody believes,
except the person who made it.
An experiment is something everybody believes,
except the person who made it."*
Albert Einstein

RESULTS AND REVIEW OF THE PAPERS

This chapter gives short reviews and summaries of the four papers which the thesis is based on.

PAPER I: REFLECTION SPECTROSCOPY OF ANALGESIZED SKIN

Previous studies^{160, 161} had revealed the occurrence of erythema in a provocation model constituting the application of an analgesic cream, EMLA, followed by local heat stimuli. The aim of this paper was to gain deeper knowledge of the occurrence of erythema and therefore a study was designed to assess changes in the chromophore content of the skin by using a spectroscopic system, see Figure 19, and relating the DRS data to the microcirculatory perfusion measured by LDPI, during moderate provocation of the microcirculation.

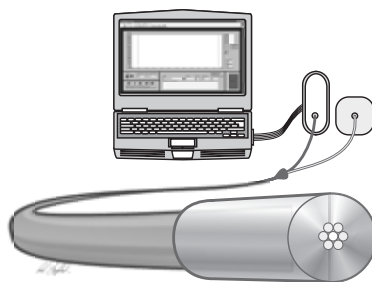


Figure 19: Schematic illustration of the system used in Paper I, consisting of a light source, a spectrometer and a probe with one receiving fiber encircled by six emitting fibers.

The provocations and measurements were carried out on the ventral aspects of the lower forearms, and in total 12 subjects were included with a loss of data in only one test subject. Measurements were carried out after five different time intervals covering 20-180 minutes of EMLA or placebo treatment. One arm was chosen for EMLA treatment and the contralateral arm was treated with a placebo cream.

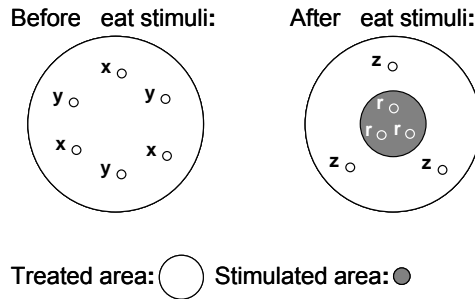


Figure 20: Schematic illustration of the measurement areas and measurement points, before and after applied heat load. The x denotes initial measurements, y denotes measurements after EMLA treatment, z denotes measurements outside of the heat-stimulated area, and r denotes measurements inside of the heat-stimulated area.

In order to study the changes of the chromophore content and tissue oxygenation, spectra were recorded before and after each provocation, see Figure 20. Baseline measurements were conducted for all sites but the long term stability of the light source proved to have too large fluctuations to enable any comparisons with the baseline measurements; while short time stability proved no problem. Instead difference spectra between affected and unaffected skin, yielding the relative increase of absorbance, were calculated and used to study the local effects of the heat provocation; 45°C during 9 seconds. To minimize the effects of the heterogeneity in the tissue three spatially separated spectra were recorded and averaged. Spectra were decomposed into relative values for the oxyhemoglobin and deoxyhemoglobin using a Beer-Lambert model and curve fitting with a resulting goodness of fit of 0.95-0.99. To be able to compare spectroscopic data with the LDPI measurements the sum of the hemoglobin derivatives were used as an estimate of the blood volume.

Areas were considered to be responding to the applied heat load if the sum of the chromophores exceeded mean plus two standard deviations of normal variations in skin. This resulted in a total of 20 responses for the spectroscopic measurements and 19 responses for LDPI measurements where the two methods corresponded in 14 of the classified responses. The number of responses increased with the

increased application time of the analgesic cream, and only two responses were found in placebo treated areas. For the spectroscopic signal it was found that the increase of oxygenized hemoglobin was prominent being six times higher compared to that of deoxygenized hemoglobin.

By calculating the difference spectra between two adjacent areas, measurements r and z , see Figure 20, the erythematous response from normal skin was discerned. This approximation could be dubious since the inflammatory response of the erythema might actually be causing additional changes in the optical properties not originating from the hemoglobin response. However, the difference spectra will give the total response of the applied stimulus as well as the change in the optical properties as a whole; similar approaches has been proposed by others^{162, 163}. Furthermore, the study was carried out not to examine the optical properties in detail but to study the effect of the stimulus and the results thereof.

The results of the analysis were convincing considering the high goodness of fit, and can thus be regarded as giving a fair indication of the response. Absolute values can, however, not be discussed using this approach. It can be concluded that the response due to the treatment with analgesic cream followed by heat provocation can be characterized as a localized increase of oxygenized hemoglobin.

PAPER II: A DIFFUSE REFLECTANCE SPECTROSCOPIC STUDY OF UV-INDUCED ERYTHEMATOUS REACTION ACROSS WELL-DEFINED BORDERS IN HUMAN SKIN

In Paper II the aim was to study the border zone of UV-induced erythema in human skin by DRS measurements. The motivation for this study was the use of a modified phototesting protocol based on a spatially varying UV-field.

Phototesting is traditionally performed by applying a range of increasing doses of UV-radiation to an individual. The minimal erythema dose (MED) is then decided as being the lowest dose possible which induces a visually discernable erythema. To improve the sensitivity of the MED assessment and to gain dose-response data, a provocation using a divergent beam has previously been proposed where the MED is estimated by the diameter of the erythematous response¹⁶⁴. Being able to measure erythema changes over a skin area is a prerequisite for the specific phototesting protocol.

The MED assessment for this protocol is normally performed by visual inspection and geometric measurements using a ruler, or by

analyzing an LDPI image. However, spectroscopic measurements are considered to be both more sensitive and more objective than visual inspection and could therefore be advantageous. At the same time the chromophore content and skin oxygenation data obtained by DRS are complementary to the blood perfusion data measured by LDPI thus elucidating more and new aspects of the response.

The UVB-provocation was performed by illuminating a circular area (\varnothing 15 mm) with different exposure times, ranging from 0 to 12 seconds, thereby creating a series of increasing UV-doses varying between 0 and 168 mJ/cm². To create a sharp border between irradiated and non-irradiated tissue a demarcated, unaffected zone was created by a 3 mm wide black tape, opaque to UV-radiation, in the middle of the provocation area. The non-irradiated test site (0 seconds) was used as a reference area for estimation of normal variation on an individual basis. Ten individuals were first enrolled and the volar forearms were chosen as provocation site. A commercially available spectroscopic system, see Figure 21, was used for the readings of the reactions 6 and 24 hours after provocation.

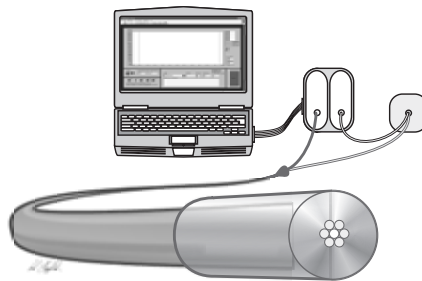


Figure 21: Schematic illustration of the system used in Paper II, consisting of a light source, a two-channel spectrometer and a probe with one receiving fiber encircled by six emitting fibers.

To achieve repeatable measurements a robotic system was used, for movement of the probe from one skin site to another. The robotic system has high precision in its ability to perform scan lines with fixed stepping length between two measurement points and exerts a negligible pressure on the skin surface. Due to the probe configuration with a single receiving fiber (\varnothing 0.2 mm) and 6 emitting fibers encircling the receiving fiber, a step length of 0.2 mm was chosen. The scanning of the border zones was done perpendicular to the demarcation zone in two separate scan lines of 35 measurement points with a total scanned distance of 6.8 mm. Since the border zone was of interest in this study only visibly discernable provocations were chosen for DRS measurements.

A modified Beer-Lambert model and curve fitting in least square sense was chosen to estimate the chromophore content from the spectral data in the wavelength range of 500 to 700 nm. Included in the model were oxyhemoglobin, deoxyhemoglobin, eumelanin, pheomelanin and in addition a baseline plus a variable slope to compensate for scattering in the tissue. The sum of the two hemoglobin derivatives was then used as the erythema predictor. To classify a tissue as being erythematous, a criterion using the mean plus two standard deviations of the reference site was chosen.

The profiles of the chromophore content vs. the line scan showed large variations along the scan line for both normal and affected tissue, see Figure 22. The result of the decomposition, goodness of fit for average $R^2 \sim 0.95$, showed that the increase was mostly due to oxyhemoglobin. No discernable variations in the melanin content were found and the melanin factors were almost exclusively due to pheomelanin.

The border zones were estimated by a least square fitting of a linear function between the maximum value in provoked areas and the minimum in the unaffected area, resulting in an approximation of the derivative, or slope, for the border zone, see Figure 22.

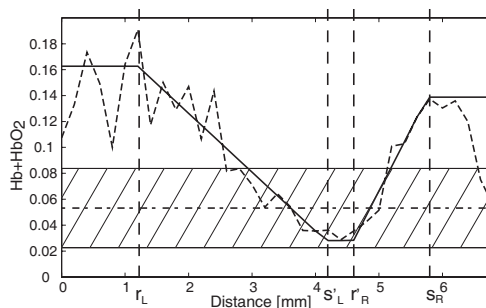


Figure 22: A scan line showing the estimated hemoglobin content, dashed line and the approximated profile, solid line. Hatched area indicates the mean ± 2 standard deviations.

The results of the scanning procedure and classification resulted in a total of 137 border zones analyzed. The estimated width ($M \pm SD$) for the left and right border zone was calculated to be 1.81 ± 0.93 mm and 1.90 ± 0.88 mm respectively. The unprovoked area between the left and right slopes was estimated to be 0.77 ± 0.68 mm. The results showed large variations compared to the sharp border zones expected and the demarcated region was less than half the width of the strip.

In conclusion, the chosen model was adequate to provide spatially distributed data for the chromophore content along a scan line thus characterizing the borders zones. However, the spectroscopic system was suboptimal resulting in a probable overestimation of the border zone.

PAPER III: MYOCARDIAL TISSUE OXYGENATION ESTIMATED WITH CALIBRATED DIFFUSE REFLECTANCE SPECTROSCOPY DURING CORONARY ARTERY BYPASS GRAFTING

In Paper III the task of measuring tissue oxygenation during the difficult and complex situation of open chest surgery was approached. The aim of the study was to develop a calibrated DRS system for assessment of myocardial tissue oxygenation during Coronary Artery Bypass Grafting (CABG), encompassing a complex measurement situation. To be able to study the relationship between measurements proximal and distal in relation to a stenosis we aimed at getting absolute tissue oxygenation values for the investigated tissue. To achieve this, the variations of the optical properties in the myocardial tissue had to be taken into consideration.

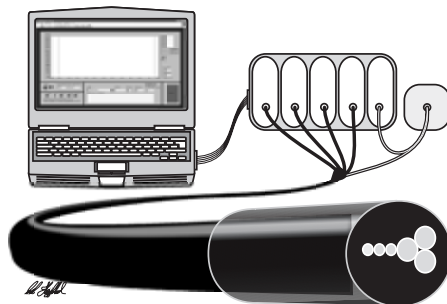


Figure 23: Schematic illustration of the system used in Paper III, consisting of a light source, a five channel spectrometer and a probe with five different source-detector distances.

The chosen approach was based on a modified Beer-Lambert model taking both the absorption and the scattering into account. The light transport algorithm used was originally proposed by Jacques et al.¹⁴⁵ for measurements of esophageal tissue and horse sarcoids, but modified to suit measurements of the human heart. The analysis of chromophores included oxyhemoglobin, hemoglobin, lipids and water; where hemoglobin absorption was used to represent both the hemoglobin and the myoglobin due to their resemblance in absorptivity, but no cytochrome spectra were included. The curve fitting was approached in two steps. First the scattering was estimated in a region where absorption was low. Secondly the

absorption and oxygen saturation was estimated in the wavelength band where the most prominent absorption of hemoglobin can be found.

In addition to the algorithm, the improvement in this study was the calibration of the probe and algorithm against an extensive grid of 56 optical phantoms. The grid consisted of different mixtures of absorbers and scatterers, spanning over absorption coefficients from 1 to 288 mm^{-1} and scattering coefficients from 200 to 1000 mm^{-1} . In addition, the probe was purposely designed to measure different tissue volumes by arranging the optical fibers geometrically allowing four separate source-detector distances, see Figure 23. The probe had to be sterile during measurement sessions and it was therefore impossible to incorporate a standard procedure including white reference recordings in connection to the measurements. Reference measurements were therefore recorded using a solid reference phantom at the end of each measurement, and the light source was continuously monitored by one dedicated channel of the spectrometer. To compensate for any difference in coloration of the reference phantom a normalization algorithm was developed, relating all measurements to reference measurements on a PTFE tile.

The severity of the surgical procedure dictated to some extent the design of the measurement protocol to limit the time taken from the surgeon. Nevertheless the study incorporated temporal measurements during interesting dynamic phases as well as spatial measurements in the vicinity of the stenosis. The measurements were furthermore distributed over time incorporating five different phases; before aortic cross-clamping (baseline); after aortic cross-clamping and cardioplegic infusion (postcardioplegic infusion); before the release of the aortic crossclamp (prereperfusion); after the release of the aortic crossclamp (postreperfusion) and after surgery when the extracorporeal circulation is completely phased out (postCABG).

In total 14 subjects were first included and a total of 10 subjects were investigated in the final analysis. The temporal measurements proved promising results in the initial analysis but movement of the probe in relation to the heart induced severe artifacts and the analysis was concentrated towards the spatial measurements. Similarly the different source detector distances could not be analyzed due to too low SNR values. Excessive fat on the heart muscle was found in two subjects where no discernable hemoglobin could be found.

The curve fit was satisfactory with an average R^2 for the distal recordings of 0.96, ranging from 0.86 to 0.99. The oxygen saturation

results yielded that the tissue oxygenation was significantly higher for postcardioplegic infusion and postreperfusion than at baseline measurements, and borderline significantly higher comparing postreperfusion with prereperfusion measurement. Individual comparisons of distal data showed that tissue oxygenation increased during aortic clamping versus baseline in 7 out of 10 cases. Tissue oxygenation decreased in 6 out of 10 cases during cardiac arrest, but increased in 7 out of 10 cases after reperfusion. Finally, tissue oxygenation increased in 8 out of 10 cases for comparisons between postreperfusion and baseline measurements. For the proximal measurements 5 out of 5 cases showed increased tissue oxygenation during aortic clamping and cardioplegic infusion, and in 4 out of 5 cases the tissue oxygenation increased comparing postreperfusion versus baseline.

In conclusion, a method was presented for estimating the oxygenation of heart tissue using a calibrated probe with source-detector distances less than 1 mm. The light transport algorithm used analyses the measured spectrum by the use of a model, including both scattering and absorption effects in the tissue. The estimated model proved to be in good agreement (average $R^2 = 0.96$) with the measured DRS spectra. Hence the proposed method was proven to function satisfactorily in the operating theater during bypass surgery, despite the complex measurement situation.

PAPER IV: VISIBLE, HYPERSPECTRAL IMAGING EVALUATING THE CUTANEOUS RESPONSE TO ULTRAVIOLET RADIATION

In Paper IV a newly designed hyperspectral imaging system, based on spectral scanning, was presented. The capacity of the system was tested by using a well documented phototesting protocol. The provocation was chosen because of its diversified effects on the skin covering both spatial effects, e.g. sharp and diffuse erythema, as well as gradual changes over time including different chromophore responses, i.e. hemoglobin and melanin. The measurements were chosen to maximize the test of the hyperspectral system.

The design of the system was based on commercially available components. The HSI-system consisted of a CCD-camera, an optical lens, and a liquid crystal tunable filter. The light source consisted of 384 white LEDs arranged in a matrix illuminating the tissue uniformly via a semi-transparent mirror. The spatial resolution of the system was limited by the system's optical zoom and the specifications of the CCD-array but was able to record images of 520×696 pixels over a rectangular FOV covering a tissue area of 38×29 mm. The spectral resolution of the LCTF, defined at full width

half maximum, was 10 nm over the wavelength range from 450 to 720 nm.

The provocation was made by a range of different UVB-provocations; three different doses administered to three skin areas; a spatially varying provocation and a provocation with a sharp border zone. To diversify the measurements even further, three subjects with different skin types were selected under the assumption that they would elucidate the tests by three different responses. Measurements were scheduled at five different occasions when response changes were expected.

For the analysis of the spectra in the recorded hypercube, we adopted the approximative approach of a basic Beer-Lambert model and linear regression to mimic the analysis of former studies incorporating the main chromophores of the skin. Intensity variations in the recorded hypercubes made it necessary to include a baseline in the fitting model, to compensate for these variations which could be attributed to scattering. Before any measurements in vivo, original absorption spectra were recorded of the hemoglobin derivatives to test the system in a basic way but also to compare the measurements to documented reference spectra. This extensive work resulted in satisfactory results for oxyhemoglobin and deoxyhemoglobin comparable to typical reference spectra found in the literature¹⁰⁶. After spectral analysis the data from the hypercube were decomposed into separate images of the three chromophores based on the results from the curve fitting. A fourth residual image was produced to visualize any spatial variations of the error between fitted spectra and measured spectra. Analysis of the error image, R^2 , gave a good fit of 0.95-0.97, in contrast to areas that were not physiological, i.e. pen markings, where the R^2 -value was as low as 0.70. Since only relative values could be estimated, tissue in the provoked areas had to be compared with unaffected tissue giving relative values for any chromophore increase above average of normal skin.

The dose response test¹⁶⁴ using divergent UV-irradiation resulted in a graded increase of oxyhemoglobin, closely resembling the applied UV-field. Further, subject II showed a higher relative increase compared to subject III, which could be expected from the difference in skin types.

Initial erythema development was measured over time and the response was compared to the surrounding tissue in order to find the relative increase of oxyhemoglobin. These results revealed a fast initial response that leveled after six hours, and still was present 24 hours after provocation. For test subject I, with corresponding skin

type I, there was even a discernable change of the response diameter for the first six hours.

The effect of the size of the provocation field on the response magnitude was evaluated by comparing the quotients between the different responses. These results were ambiguous since the largest area was not the most prominent contradictory to the expectations. However the expected relationship could be discerned for the two smaller provocations. A further lack of consistency was that subject II had no apparent response for the largest provocation area.

Characterization of the abrupt erythema border was done by differentiation across a chosen strip of the provocation in the image of oxygenized hemoglobin distribution. The differentiation was possible due to the large number of measurement points in the image and it was found that the abrupt border had a higher derivative than that of the gradual provocation as expected.

A relative increase of the melanin content in the provoked area in comparison with unprovoked areas was found for subject III. However, subject II did not present any increase of melanin after the provocation. Nevertheless it was possible to identify natural pigmentation heterogeneities, such as freckles, as well as individual hair shafts as compared with visual inspection.

In summary, satisfactory fitting results were achieved and the system was able to yield expected results of different effects after provocations with UVB-radiation. It was thereby possible to study spatially and temporally resolved chromophore changes by using well-defined doses and geometries for the UVB-provocations. Further evaluation is needed and it is necessary to improve the underlying model, introducing scattering, and the calibration of the system. Being an imaging technique it can be expected that pure image analysis can enhance the interpretability of the results.

10

*"If you shut your door to all errors,
truth will be shut out."
Rabindranath Tagore*

DISCUSSION AND CONCLUSIONS

This thesis involves the development and evaluation of spectroscopy measured in a single point using fiber optic probes to the use of a hyperspectral imaging system. The systems have been used to measure relative and absolute concentrations of tissue chromophores in the microcirculatory bed, specifically on human skin and heart. The physiological situations have been: evaluation of the microcirculatory response in relation to local heating and application of analgesic cream, Paper I; evaluation of the chromophore content and change in tissue oxygenation in skin exposed to UV, studying the boundary between exposed and non-exposed tissue, Paper II; the tissue oxygenation of the heart in relation to important surgical stages during coronary artery bypass surgery, Paper III and the spatial distribution of UV-response over time using HSI, Paper IV.

METHODOLOGICAL AND MODEL CONSIDERATIONS

Curve fitting has been used throughout Papers I-IV to fit various models based on Beer-Lambert law to find the coefficients for the different chromophores hidden in the measured DRS spectrum. Wide wavelength band spectra, instead of using a few wavelengths, have been used in order to suppress the influence of random or stochastic noise in the measured spectra. Additionally, the calculations have been straightforward and proven to assess the measured spectra satisfactorily despite simplified models and this was proven by the high goodness of fit for all setups. However, the uncertainty level due to relative values forced a wider criterion for classification to encompass any deviations of the true absorbance as

compared with the apparent absorbance used. Therefore a criterion of two standard deviations was chosen to incorporate 95% of normal variation in the chromophore content, if a normal distribution can be assumed. However, the use of such a high threshold in the relative values can induce false negative classifications since large variations are needed before being classified as responding. The selected criterion will thus have an impact on the results, especially if the outcomes of the predicted values are sensitive to threshold level adjustments.

A Beer-Lambert model was used for analyzing the DRS signal in Paper I but with the assumption that any difference due to scattering and bulk absorption is cancelled out or minimized by calculating the difference between responding and non-responding sites. Spatial variations in the optical properties are reflected in the DRS signal and further limited by averaging of three spatially distributed and independent measurement points, minimizing the influence of heterogeneous scattering effects. Good fits were achieved despite the fact that no scattering compensation was performed. Hence it can be assumed that the normalization of the intensities and the use of difference spectra have diminished the influence of the scattering effects. Others have also used similar approaches to calculate the apparent absorption successfully^{163, 165}. Still, the main purpose of this study was to classify and characterize the responses showing that both the analysis and the rough approximations proved sufficient.

Scattering effects were addressed through a modified Beer-Lambert model, in Paper II, as suggested by Meglinski and Matcher³⁴. This model assumes that the scattering effects on the absorbance can be described as a baseline and a wavelength dependent slope. This approximation of the scattering effects proved sufficient for analysis of a border zone. However, scattering might still have an impact on the absorbance analysis in Paper I-II, as this type of models does not fully account for nonlinear scattering effects.

Absorption in tissue can never be estimated in absolute values unless scattering and photon pathlength are taken into account. However, relative values that are proportional to both the absorption and the photon pathlength, i.e. $\mu_a \cdot l$, are possible to achieve with models that diminish the effects of scattering. This can be done by subtracting measurements where the scattering effects, G , is canceled out; or by modeling G as a linear wavelength dependent function, $\delta + \gamma \cdot \lambda$, in the curve fitting. The first approach was used in Paper I and the latter in Paper II. For Paper III, a more complex light transport model was introduced. This model, which includes a more refined description of how scattering affects the light transport, was calibrated using

known optical phantoms. As a result, solutions using this model yielded absolute values of chromophore concentrations. Finally in Paper IV the scattering term was identified as a baseline offset, with no wavelength dependence.

The short source-detector distance in the probes used, approximately 200 μm , is suitable for microcirculatory measurements, as the main contribution to the signal will originate from epidermis and the upper part of dermis¹⁶⁶. For this type of setup, where the photon pathlength is short, a high degree of absorption is needed to be able to detect any absorption related intensity attenuation. Therefore, the wavelength band 500-600 nm is suitable for estimating blood concentration and oxygenation. However, for a short source-detector separation the analysis becomes susceptible to scattering effects which calls for more advanced models that accurately describes the impact of scattering. The effect of scattering can be minimized by choosing a separation of about 1.7 mm; a separation where scattering has a minimal influence on the detected intensity¹⁶⁷.

In studies of the heart tissue, Paper III, absolute values were of necessity to correctly assess the microcirculatory state of the heart to indicate changes during surgery. Therefore, a light transport model taking the optical properties into account was used during open chest surgery. In this setup the scattering was accounted for by a refined, Beer-Lambert, transport model and the calibration of the probe against phantoms with known optical properties. Using the calibrated probe it was possible to estimate the optical parameters in the tissue and therefore the true absorbance. The absolute values and fractions of the chromophores can thus be compared between sites and individuals, independently of any difference in the optical properties in the tissue. This allows for more strict comparisons through correction of the change in pathlength and attenuation due to scattering in the tissue.

A similar approach has been proposed by Doornbos et al.⁴⁰, where the diffusion approximation was used in combination with spatially resolved measurements. The method presents good results for wavelengths longer than 600 nm. This method, however, used fiber-separations longer than 1.75 mm which is in contrast to the probe design in Paper III which had a maximal fiber-separation distance of 1.2 mm; where a shorter separation distance is more suited to study effects in the microcirculatory compartments. In the present setup a spatially resolved analysis as described in Larsson et al.¹⁶⁸ could not be implemented due to low light intensities for longer fiber separations. Foremost because of the setup of the spectrometer using 100 μm slits for the fibers with the two largest source detector

distances, it was not optimal for recording as much light as needed. Therefore, the single distance method presented by Jacques et al.¹⁴⁵, was attractive since it allows for a simpler implementation of the software, despite a rather extensive calibration using a phantom grid. An interesting application has also been presented by Amelink et al.^{43, 169} that uses a technique called differential pathlength spectroscopy that makes use of a short source-detector fiber distance to detect the most superficial tissue layer which can be an alternative method to study microcirculatory phenomena.

To improve the fitting procedure of the recorded DRS spectra and the light transport model in Paper III, the scattering approximation, Equation 29, was normalized with an arithmetic constant wavelength of 700 nm, a value in the middle of the analyzed wavelength band. This was not used in the original article¹⁴⁵ but something we later discovered increased both the algorithm solving speed and robustness with no identifiable drawback. This normalization procedure has also been suggested by others¹⁷⁰. Furthermore, the fitting procedure was split into two wavelength regions. The higher band with wavelengths above 700 nm, where scattering is dominant, was used to find the reduced scattering coefficient of the tissue. The lower wavelength band was aimed at finding the fraction of hemoglobin and the oxygen saturation, where hemoglobin absorption is dominant.

The HSI-system, Paper IV, used a modified Beer-Lambert approximation, including only a constant baseline that was identifiable as the scattering term, δ , described by Meglinski³⁴, Equation 25, thereby approximating the scattering. Others have proposed this approximative model for the analysis of hyperspectral images and proved it successful^{158, 159}. Further, the focus in Paper IV was on system development and evaluation. Therefore, the speed of calculations enabling relative values was prioritized rather than finding absolute values. The approximative model gave satisfactory results without introducing any large spatial variations in normal tissue. Additional scattering effects will be addressed in the future. However, the inclusion of melanin in the model might have compensated for wavelength dependent scattering effects, as both melanin and scattering can have similar influence on the absorbance¹²³. Being an imaging modality, the curvature of the tissue possibly has to be taken into account, and in Paper IV the influence of non-planar surfaces was avoided by flat surfaces, selecting the best possible, at the volar side of the forearms. The effects of the curvature will be addressed in the future. Further, there was no

direct correction for specular reflection except for the choice of the light source, which produces diffuse light.

In Paper I, II and IV the wavelength region analyzed has been limited to a subband ranging from 500-700 nm thereby simplifying the analysis. This has implied that the need for including chromophores other than hemoglobin derivatives and melanin has been limited due to their dominant absorption. However, in Paper III a broader wavelength range was used which prompted for the inclusion of chromophores such as water and fat in the model. Deviations between the model and the measurements were nevertheless found. No additional chromophore could be found by analysis of the residual spectra. Possible candidates may nevertheless be methemoglobin or metmyoglobin and cytochrome aa₃, based on the appearance of the spectra where discrepancies were found in the region around 520 and 630 nm. Some discrepancies found are thus possibly due to the fact that too few chromophores were used, and it might be rewarding to include carotene, bilirubin, cytochromes and methemoglobin in future models. However, the presence of these chromophores varies for different body sites and between individuals and the concentration is usually low making them difficult to detect. Still, the 1% of metmyoglobin, normally seen in healthy subjects, could possibly have an influence on the absorption around 630 nm and therefore be detectable. In the model the absorption of hemoglobin and myoglobin was also combined by their sum since no differentiation of the chromophores was expected to be found. Others^{171, 172} have reported such a differentiation therefore a closer investigation might be needed, but since myoglobin spectra are red-shifted by only a couple of nanometers; this will make it difficult to analyze by using a decomposition algorithm only, yet others have succeeded¹⁷³. In addition, it has been suggested that in the clinical setting there is no real use in differentiating the myoglobin in the measurements since hemoglobin deoxygenation is the earliest detectable sign indicating severe conditions in the tissue. However, a change in myoglobin will only be detectable later⁵¹. The degree of oxygenation of cytochromes and myoglobin may still be interesting from a researcher's point of view.

One way to test a technique in practice is the use of well-defined models, in theory, by phantoms, or in vivo measurements, for evaluation and feasibility studies. In this thesis only in vivo provocation models have been used but phantoms with known optical properties have been used to calibrate probes for better estimation. The advantage with the in vivo approach is that any situation and reaction is real and presents as complex measurement

as can be, and if the method can yield plausible results in such conditions then it has proven worthy. The disadvantage is the complexity of the model and lack of control for all parameters that may have influence on the recorded signal making the results difficult to explain. Nevertheless, it can be used to study the effects of well-defined provocations and in combination with other methods it is possible to form hypothesis about the recorded signals. For example, in Paper I the use of LDPI together with DRS was combined using the same in vivo model as had been used before; at that time the flow and capillary density was measured¹⁶⁰. It can possibly be beneficial to combine different techniques to study the functional response in a tissue volume thereby predicting and estimating the responses better and bringing forth new possibilities to understand the light-tissue interaction, experimentally and clinically.

PHYSIOLOGICAL ASPECTS

Penetration of visible light in skin tissue is wavelength dependent where the blue light is restricted to the upper part of the skin as compared with red wavelengths⁸⁶. The shallow penetration of visible light in lower wavelengths enables a smaller sampling volume covering foremost microcirculatory vessels close to the tissue surface. This is of interest since the microcirculation is necessary for tissue health and survival. A continuous high blood flow is not enough to ensure healthy tissue. If no oxygen reaches the cells they will eventually die even if a high flow can be found present in the tissue as a whole; erythromelalgia¹⁷⁴ and the diabetic foot¹⁷⁵ are pathologic examples of this phenomenon. A typically critical situation can be found in the heart where ischemic conditions or abnormal loss of blood perfusion almost immediately result in a loss of functionality. A prolonged ischemia will also result in cell death starting after such a short time period of only 15 to 50 minutes¹⁹. The heart ischemia is of course difficult, if not impossible, to measure in practice due to the placement of the in vivo heart. In experimental settings, however, the use of spectroscopic techniques can be useful to gain deeper knowledge about the microcirculatory effects during, and the mechanisms behind, ischemic conditions in the heart as well as it can be indicative for the reperfusion of the heart.

A prolonged mismatch between supply and demand, not only for the heart but for all tissues, will lead to disturbances in the tissue functionality and ultimately necrosis^{2, 12}. This is partly due to a limited inflow but can also be an effect of the decreased outflow resulting in a harmful decrease in the pH-values of the tissue¹². Even for other tissues capillary occlusion for longer than an hour can

result in irreversible damages. The mismatch between supply and demand may also occur due to a sudden increase of the demand in the tissue by, for example, injuries and inflammatory responses^{1, 2}. Therefore, a need to identify these conditions is apparent and it can be addressed by spectroscopic measurements¹ utilizing short source-detector distances and small sampling volumes, as has been used in Papers I-III, and possibly detecting hemoglobin and myoglobin derivatives and cytochromes.

Furthermore, a measurement in a single point, with or without a known sampling volume, can not be used as an estimate of the state of the tissue as a whole. However, if the local tissue is in need, and the microcirculation is not able to meet this demand locally, then it is probable that areas, or compartments, exist with the same type of need. Conversely, the assumption that if the systemic circulation is high then the metabolic state in the peripheral tissue is also functioning well is equally wrong. In fact it is possibly more likely to assume falsely that the tissue is in a healthy state by looking at systemic variables, but where the nutritious flow is restricted, or non-existent, which leads to undetected ischemia¹². Spectroscopy can be used to differentiate between these kinds of conditions by studying the ratios of oxygenized and deoxygenized hemoglobin, Papers I-III, giving an indication of the metabolic surroundings near the cells in the sampling volume. The spectroscopic analysis is not limited to analyzing the functional hemoglobins but also dyshemoglobins can be detected making it possible to measure functional oxygen saturation. If furthermore an HSI-system as presented in Paper IV, is used then it is possible to assess the metabolic state covering larger areas in a shorter amount of time, thereby enhancing the possibility to identify the state of a tissue not just on a microscopic scale but also on a macroscopic scale, which has also been presented¹⁷⁶. If, further, the pathologic conditions can be characterized by the HSI-system then this will enable delineation between healthy and pathologic conditions in an instant.

The results in Papers I, II and IV show a predominant oxyhemoglobin response in the developed erythema, which is in accordance with findings of others¹⁷⁷. Melanin assessment has proved more difficult. In Paper I no melanin was expected due to the nature of the difference spectra, canceling the melanin effects. No increase in the melanin factors was found following UVB-provocation in Paper II, probably due to the fact that measurements were carried out 24 hours after provocation reducing the possibilities of a delayed tanning, which normally has an onset after 72 hours¹²². Further, the decomposed melanin content was almost exclusively

due to pheomelanin, which might be an estimate of the true situation since all subjects were Caucasian. The low and sometimes nonexistent values for eumelanin, however, indicate that the result for melanin could be artifactual. This was possibly due to the scattering term that varies with wavelength, but also due to the similarities between absorptivity spectra for the two melanin derivatives. In Paper IV, however, a localized increase of melanin was found, 336 h after UVB- irradiation, which could be attributed to the applied provocation. Presence of local spots of melanin in the skin, identifiable as freckles, could also be found and verified by visual inspection. The approximate compensation for scattering and the scattering behavior of melanin can of course have introduced the artifactual presence of melanin. The extent of any such cross-talk will be addressed in the future. However, the identifiable melanin content indicates the possibility to detect melanin, at least in higher concentrations.

FUTURE DIRECTIONS

The combination of refined theoretical models and well-defined physiological models, along with physiological provocations, is probably the best way to proceed in order to characterize tissue and develop the DRS technique further. The whole process being iterative with theoretical models predicting the behavior of light propagation and tissue interaction and the differences found in the measurements, after provocations, will force the theoretical models to be improved when compared with reality.

Further, if the imaging technique can be adopted to take scattering effects into account yielding absolute values, this could be beneficial and used for fast screening to find normal heterogeneities in the tissues and delineate any irregularity due to pathologic conditions. In addition, the instruments must be further improved in order to shorten acquisition times, improve the accessibility, improve the algorithms and ultimately achieve measurements with high specificity and sensitivity, to reach the clinical setting where a need exists for microcirculatory assessment.

CONCLUSION

The use of diffuse reflectance spectroscopy in this thesis includes a range of models based on the Beer-Lambert law. Analyzing relative changes in absorbance diminish the influence of scattering effects. Further, if the analysis is performed on a single spectrum, scattering is accounted for by a linear function approximation. From these assumptions, estimates of relative absorption were calculated, i.e.

absorption \times pathlength. A more advanced light transport model and a calibrated probe were used to assess the optical properties in tissue, thus yielding absolute chromophore concentrations.

Uncalibrated models were used to analyze the relative changes in skin chromophore concentration in response to external provocations such as local heating and UV irradiation. The calibrated model enabled studies of myocardial oxygenation changes during bypass surgery. This model refines the conclusions of inter- and intra-individual measurements, which objectify measurements in more complex situations. The achieved stricter comparison of different physiological states makes it possible to discern minute differences that could be of importance for tissue diagnosis.

The experimental and clinical measurements have evolved from single point measurements, via linear mechanical scanning using single point spectroscopy to spectral imaging, presenting a possibility of spatial analyzes of the chromophore content in the tissue.

In summary, advancing from a restricted Beer-Lambert model, diminishing scattering effects, into a Beer-Lambert model taking optical properties into account, chromophore estimation algorithms have been refined progressively. This has allowed the advancement from relative findings of chromophores to absolute values. Further, the development of a hyperspectral system has improved the analysis of chromophores by adding another dimension.

11

*"Truly great friends are hard to find,
difficult to leave,
and impossible to forget."
Unknown*

ACKNOWLEDGMENTS

The time has come to put an end to a long and winding journey. I would never have done this journey without a lot of persons and hopefully I will give full credit to you all. I have been here for so long that I almost consider the department to be my second home, and thereby regard all employees and colleagues, former and present, as part of my second family.

First of all goes my gratitude to my supervisor Göran for letting me do this journey and taking me to places I would never have dreamt of, both scientifically and also geographically. Thank you for your support and trust! My co-supervisor Tomas also deserves special mention for his support and for providing interesting and challenging projects.

Gert and Karin, along with all colleagues at BIT – thanks for providing a friendly and inspiring scientific environment.

To all my co-authors: Marcus, Mikael, Tomas, Göran, Henrik, Michail, Chris, Tobias, Daniel, and Henrik – thanks for the scientific discussions and friendly atmosphere. Without you, there would be naught.

All former and present colleagues at the department that has been a part of my life as a PhD student, I will remember you all.

However, some of you deserve special mention; some of you are colleagues of the Old School and some are New Kids on the Block: Mikael, for teaching me all you know and introducing me to LHC; Michail, for teaching me the good life and for being my soulmate at

the department; Daniel, for showing me the good life and always pushing for that little extra, ever since we were students; Marcus, my bike buddy, for times of joy and work; Marcus, my first laboratory partner and companion to Middle Earth; Tobias, my last laboratory partner, for a shared interest in calves; Håkan, for support in my studies of light and sound; Mats, who never says die; Ingemar for fruitful discussions about sport and optics; Christer and Amir, the Criss and the Cross of IMT that will make you...

Life at the department would have been boring without you guys!

I should not forget the TA-staff, without you my work would not have been possible and not as fun either. Ta ta!

International connections must be mentioned: Bill, my American connection (who is a freakin' genius); Cecile and Frank, my Dutch connections; Moa[‡] my Latin connection and all my Norwegian nabor.

All friends outside of IMT, who joined me in doing the stuff I really like and which I did not think was possible. Thanks for always trying to save me from Karōshi; not that I ever was in any real danger. Except, perhaps, at the end...

Finally my gratitude goes to those I could never be without:

My sister Anna and her family, Mikael, Johan, and Julia, for embracing me and letting me take part in their lives.

My mother, Ann-Christin, and father, Einar, for believing in me especially when I doubted myself but also for making me who I am. Tack för allt!

Elisavet, for everything, but foremost for being you,
you make me smile – You are my Everything.

REFERENCES

1. M. Siegemund, J. van Bommel and C. Ince, "Assessment of regional tissue oxygenation", *Intensive Care Medicine*, 25(10), 1044-1060, 1999.
2. G. W. Schmid-Schönbein, "Analysis of inflammation", *Annual Review of Biomedical Engineering*, 8, 93-151, 2006.
3. I. Newton, "A New Theory About Light and Colors (Reprinted from Philos Trans R Soc London, Pg 3075-3087, 1672)", *American Journal of Physics*, 61(2), 108-112, 1993.
4. H. F. Bunn and B. G. Forget, *Hemoglobin: molecular, genetic and clinical aspects*, pp. 690, Saunders, Philadelphia, 1986.
5. D. W. Ball, *The basics of spectroscopy*, pp. 122, SPIE Press, Bellingham, Washington, 2001.
6. E. A. Edwards and S. Q. Duntley, "The Pigments and Color of Living Human Skin", *American Journal of Anatomy*, 65(1), 1-33, 1939.
7. V. K. Hughes, P. S. Ellis and T. Burt, "The practical application of reflectance spectrophotometry for the demonstration of haemoglobin and its degradation in bruises (vol 57, pg 355, 2004)", *Journal of Clinical Pathology*, 57(8), 896-896, 2004.
8. L. L. Randeberg, E. B. Roll, L. T. N. Nilsen, T. Christensen and L. O. Svaasand, "In vivo spectroscopy of jaundiced newborn skin reveals more than a bilirubin index", *Acta Paediatrica*, 94(1), 65-71, 2005.
9. G. N. Stamatas, B. Z. Zmudzka, N. Kollias and J. Z. Beer, "In vivo measurement of skin erythema and pigmentation: new means of implementation of diffuse reflectance spectroscopy with a commercial instrument", *The British journal of dermatology*, 159(3), 683-690, 2008.
10. G. J. Tortora and S. R. Grabowski, *Principles of anatomy and physiology*, pp. 986, HarperCollins, New York, 1996.
11. S. Mellander, *Perifer cirkulation: blodkårlens fysiologi*, pp. 177, Sandoz, Täby, 1983.
12. R. M. Hardaway, *Capillary perfusion in health and disease*, pp. 273, Futura, Mount Kisco, N.Y., 1981.
13. W. S. Beck, ed. *Hematology*. 5. ed. Vol. 1991, MIT Press: Cambridge, Massachusetts. p. 667.
14. R. L. Bick, J. M. Bennet, R. K. Brynes, M. J. Cline, L. Kass, G. Murano, S. B. Shoet and P. C. J. Ward, eds. *Hematology : clinical and laboratory practice*. Vol. 1. 1993, Mosby: St.Louis. p. 3-852.
15. I. M. Freedberg, A. Z. Eisen, K. Wolff, K. F. Austen, L. A. Goldsmith, I. S. Katz and T. B. Fitzpatrick, eds. *Fitzpatrick's dermatology in general medicine*. 5 ed. Vol. 1. 1999, McGraw-Hill: New York; London. p. 1659.
16. P. G. Agache and P. Humbert, eds. *Measuring the skin*. Vol. 2004, Springer: Berlin Heidelberg. p. 784.
17. T. J. Ryan, "Cutaneous Circulation", in *Physiology, biochemistry, and molecular biology of the skin*, L. A. Goldsmith, ed. 1991, Oxford University Press: New York. p. 1019-1084.
18. P. L. Williams, R. Warwick, M. Dyson and L. H. Bannister, eds. *Gray's Anatomy*. 37 ed. Vol. 1989, Churchill Livingstone: Edinburgh. p. 1598.
19. A. M. Katz, *Physiology of the heart*, pp. 718, Lippincott Williams & Wilkins, Philadelphia, 2001.
20. K. T. Weber, "Cardiac Interstitium in Health and Disease - the Fibrillar Collagen Network", *Journal of the American College of Cardiology*, 13(7), 1637-1652, 1989.
21. R. W. Alexander and J. W. Hurst, *Hurst's the heart*, pp. 2602, McGraw-Hill, New York ; London, 1997.

22. K. Wei and S. Kaul, "The coronary microcirculation in health and disease", *Cardiology Clinics*, 22(2), 221-231, 2004.
23. S. M. Factor, E. M. Okun, T. Minase and E. S. Kirk, "The microcirculation of the human heart: end-capillary loops with discrete perfusion fields", *Circulation*, 66(6), 1241-1248, 1982.
24. T. Matsumoto and F. Kajiyama, "Coronary microcirculation: Physiology and mechanics", *Fluid Dynamics Research*, 37(1-2), 60-81, 2005.
25. M. J. Martin, Y. A. Wickramasinghe, T. P. Newson and J. A. Crowe, "Fibre-optics and optical sensors in medicine", *Medical & Biological Engineering & Computing*, 25(6), 597-604, 1987.
26. B. Hapke, *Theory of reflectance and emittance spectroscopy*, pp. 455, Cambridge Univ. Press, Cambridge, 1993.
27. M. A. Ilias, E. Häggblad, C. Anderson and E. G. Sallerud. *Visible hyperspectral imaging evaluating the cutaneous response to ultraviolet radiation*. in Proceedings of SPIE - Imaging, Manipulation, and Analysis of Biomolecules, Cells, and Tissues V. 2007. SPIE.
28. T. Vo-Dinh, "Basic Instrumentation in Photonics", in Biomedical photonics handbook, T. Vo-Dinh, ed. 2003, CRC Press: Boca Raton, Fla. p. 6-1-6-30.
29. J. W. Longworth, "On Light, Colors and the Origins of Spectroscopy", in The Science of Photomedicine, J. D. Regan and J. A. Parrish, eds. 1982, Plenum Press: New York. p. 21-68.
30. P. Lykos, "The Beer-Lambert Law Revisited - a Development without Calculus", *Journal of Chemical Education*, 69(9), 730-732, 1992.
31. S. J. Matcher and C. E. Cooper, "Absolute quantification of deoxyhaemoglobin concentration in tissue near infrared spectroscopy", *Physics in Medicine and Biology*, 39(8), 1295-1312, 1994.
32. S. R. Arridge, M. Hiraoka and M. Schweiger, "Statistical basis for the determination of optical pathlength in tissue", *Physics in Medicine and Biology*, 40(9), 1539-1558, 1995.
33. D. T. Delpy, S. R. Arridge, M. Cope, D. Edwards, E. O. Reynolds, C. E. Richardson, S. Wray, J. Wyatt and P. van der Zee, "Quantitation of pathlength in optical spectroscopy", *Advances in Experimental Medicine and Biology*, 248, 41-46, 1989.
34. I. V. Meglinski and S. J. Matcher, "Computer simulation of the skin reflectance spectra", *Computer Methods and Programs in Biomedicine*, 70(2), 179-186, 2003.
35. J. B. Dawson, D. J. Barker, D. J. Ellis, E. Grassam, J. A. Cotterill, G. W. Fisher and J. W. Feather, "A theoretical and experimental study of light absorption and scattering by in vivo skin", *Physics in Medicine and Biology*, 25(4), 695-709, 1980.
36. F. Bevilacqua and C. Depeursinge, "Monte Carlo study of diffuse reflectance at source-detector separations close to one transport mean free path", *Journal of the Optical Society of America a-Optics Image Science and Vision*, 16(12), 2935-2945, 1999.
37. J. Hoffmann, D. W. Lübbers and H. M. Heise, "Applicability of the Kubelka-Munk theory for the evaluation of reflectance spectra demonstrated for haemoglobin-free perfused heart tissue", *Physics in Medicine and Biology*, 43(12), 3571-3587, 1998.
38. I. Seo, J. S. You, C. K. Hayakawa and V. Venugopalan, "Perturbation and differential Monte Carlo methods for measurement of optical properties in a layered epithelial tissue model", *Journal of Biomedical Optics*, 12(1), -, 2007.
39. T. J. Farrell, M. S. Patterson and B. Wilson, "A Diffusion-Theory Model of Spatially Resolved, Steady-State Diffuse Reflectance for the Noninvasive Determination of Tissue Optical-Properties In vivo", *Medical Physics*, 19(4), 879-888, 1992.
40. R. M. Doornbos, R. Lang, M. C. Aalders, F. W. Cross and H. J. Sterenborg, "The determination of in vivo human tissue optical properties and absolute

- chromophore concentrations using spatially resolved steady- state diffuse reflectance spectroscopy”, *Physics in Medicine and Biology*, 44(4), 967-981, 1999.
41. J. S. Dam, N. Yavari, S. Sorensen and S. Andersson-Engels, “Real-time absorption and scattering characterization of slab-shaped turbid samples obtained by a combination of angular and spatially resolved measurements”, *Applied Optics*, 44(20), 4281-4290, 2005.
 42. P. R. Bargo, S. A. Prahl, T. T. Goodell, R. A. Steven, G. Koval, G. Blair and S. L. Jacques, “In vivo determination of optical properties of normal and tumor tissue with white light reflectance and an empirical light transport model during endoscopy”, *Journal of Biomedical Optics*, 10(3), -, 2005.
 43. A. Amelink and H. J. C. M. Sterenborg, “Measurement of the local optical properties of turbid media by differential path-length spectroscopy”, *Applied Optics*, 43(15), 3048-3054, 2004.
 44. M. Essenpreis, C. E. Elwell, M. Cope, P. Vanderzee, S. R. Arridge and D. T. Delpy, “Spectral Dependence of Temporal Point Spread Functions in Human Tissues”, *Applied Optics*, 32(4), 418-425, 1993.
 45. S. L. Jacques, “Time-resolved reflectance spectroscopy in turbid tissues”, *IEEE Transactions on Bio-Medical Engineering*, 36(12), 1155-1161, 1989.
 46. Z. Malacara, “Chapter 19: Incoherent Light Sources”, in Handbook of optical engineering, D. Malacara and B. J. Thompson, eds. 2001, Marcel Dekker: New York. p.
 47. G. N. Lewis, “The conservation of Photons”, *Nature*, 118(2981), 874-875, 1926.
 48. J. Mobley and T. Vo-Dinh, “Optical Properties of Tissue”, in Biomedical photonics handbook, T. Vo-Dinh, ed. 2003, CRC Press: Boca Raton, Fla. p. 2-1-2-75.
 49. A. E. Cerussi and B. J. Tromberg, “Photon Migration Spectroscopy Frequency-Domain Techniques”, in Biomedical photonics handbook, T. Vo-Dinh, ed. 2003, CRC Press: Boca Raton, Fla. p. 22-21-22-17.
 50. P. Rolfe, “In vivo near-infrared spectroscopy”, *Annual Review of Biomedical Engineering*, 2, 715-754, 2000.
 51. R. Richards-Kortum and E. Sevick-Muraca, “Quantitative optical spectroscopy for tissue diagnosis”, *Annual Review of Physical Chemistry*, 47, 555-606, 1996.
 52. A. Mahadevan-Jansen, “Raman Spectroscopy: From Benchtop to Bedside”, in Biomedical photonics handbook, T. Vo-Dinh, ed. 2003, CRC Press: Boca Raton, Fla. p. 30-31-30-27.
 53. M. E. Darvin, I. Gersonde, M. Meinke, W. Sterry and J. Lademann, “Non-invasive in vivo determination of the carotenoids beta-carotene and lycopene concentrations in the human skin using the Raman spectroscopic method”, *Journal of Physics D-Applied Physics*, 38(15), 2696-2700, 2005.
 54. S. L. Zhang, C. L. Meyers, K. Subramanyan and T. M. Hancewicz, “Near infrared imaging for measuring and visualizing skin hydration. A comparison with visual assessment and electrical methods”, *Journal of Biomedical Optics*, 10(3), 031107, 2005.
 55. T. B. Fitzpatrick, J. D. Bernhard and T. G. Cropley, “The structure of skin lesions and fundamentals of diagnosis”, in Fitzpatrick’s dermatology in general medicine, I. M. Freedberg, A. Z. Eisen, K. Wolff, K. F. Austen, L. A. Goldsmith, S. I. Katz and T. B. Fitzpatrick, eds. 1999, McGraw - Hill: New York ; London. p. 13-41.
 56. I. D. Swain and L. J. Grant, “Methods of measuring skin blood flow”, *Physics in Medicine and Biology*, 34(2), 151-175, 1989.
 57. D. Huang, E. A. Swanson, C. P. Lin, J. S. Schuman, W. G. Stinson, W. Chang, M. R. Hee, T. Flotte, K. Gregory, C. A. Puliafito and J. G. Fujimoto, “Optical Coherence Tomography”, *Science*, 254(5035), 1178-1181, 1991.
 58. J. Welzel, “Optical coherence tomography in dermatology: a review”, *Skin Research and Technology*, 7(1), 1-9, 2001.

59. B. E. Bouma and G. J. Tearney, *Handbook of optical coherence tomography*, pp. 741, Marcel Dekker, New York, 2002.
60. A. M. Zysk, F. T. Nguyen, A. L. Oldenburg, D. L. Marks and S. A. Boppart, "Optical coherence tomography: a review of clinical development from bench to bedside", *Journal of Biomedical Optics*, 12(5), 051403, 2007.
61. W. Drexler and J. G. Fujimoto, "Optical coherence tomography in ophthalmology [Editorial]", *Journal of Biomedical Optics*, 12(4), 041201, 2007.
62. A. V. Challoner and C. A. Ramsay, "A photoelectric plethysmograph for the measurement of cutaneous blood flow", *Physics in Medicine and Biology*, 19(3), 317-328, 1974.
63. J. Allen, "Photoplethysmography and its application in clinical physiological measurement", *Physiological Measurement*, 28(3), R1-39, 2007.
64. G. E. Nilsson, E. G. Salerud, T. N. O. Strömberg and K. Wårdell, "Laser Doppler Perfusion Monitoring and Imaging", in *Biomedical photonics handbook*, T. Vo-Dinh, ed. 2003, CRC Press: Boca Raton, Fla. p. 15-11-15-24.
65. K. Wårdell, I. M. Braverman, D. G. Silverman and G. E. Nilsson, "Spatial heterogeneity in normal skin perfusion recorded with laser Doppler imaging and flowmetry", *Microvascular Research*, 48(1), 26-38, 1994.
66. M. G. D. Karlsson, H. Casimir-Ahn, U. Lönn and K. Wårdell, "Analysis and processing of laser Doppler perfusion monitoring signals recorded from the beating heart", *Medical & Biological Engineering & Computing*, 41(3), 255-262, 2003.
67. K. Messmer, ed. *Orthogonal Polarization Spectral Imaging*. Progress in Applied Microcirculation, ed. K. Messmer. Vol. 24. Karger AG, Basel, Switzerland. p.
68. C. Asker, *Computer assisted video microscopy : in characterization of capillary ensembles*, pp. 64, University of Linköping, Linköping, 2000.
69. A. Bollinger and B. Fagrell, *Clinical capillaroscopy : a guide to its use in clinical research and practice*, pp. 166, Hogrefe & Huber, Göttingen ; Toronto, 1990.
70. W. Groner, J. W. Winkelman, A. G. Harris, C. Ince, G. J. Bouma, K. Messmer and R. G. Nadeau, "Orthogonal polarization spectral imaging: A new method for study of the microcirculation", *Nature Medicine*, 5(10), 1209-1213, 1999.
71. P. T. Goedhart, M. Khalilzada, R. Bezemer, J. Merza and C. Ince, "Sidestream Dark Field (SDF) imaging: a novel stroboscopic LED ring-based imaging modality for clinical assessment of the microcirculation", *Optics Express*, 15(23), 15101-15114, 2007.
72. C. Ince, "The microcirculation is the motor of sepsis", *Critical care (London, England)*, 9 Suppl 4, S13-19, 2005.
73. P. Corcuff, "In Vivo Confocal Microscopy", in *Measuring the skin*, P. G. Agache and P. Humbert, eds. 2004, Springer: Berlin Heidelberg. p. 183-193.
74. M. Binder, M. Schwarz, A. Winkler, A. Steiner, A. Kaider, K. Wolff and H. Pehamberger, "Epiluminescence Microscopy - a Useful Tool for the Diagnosis of Pigmented Skin-Lesions for Formally Trained Dermatologists", *Archives of Dermatology*, 131(3), 286-291, 1995.
75. M. Moncrieff, S. Cotton, E. Claridge and P. Hall, "Spectrophotometric intracutaneous analysis: a new technique for imaging pigmented skin lesions", *British Journal of Dermatology*, 146(3), 448-457, 2002.
76. D. A. Peredina, "Overview of Dermatologic Digital Imaging", in *Handbook of non-invasive methods and the skin*, J. Serup and G. B. E. Jemec, eds. 1995, CRC Press: Boca Raton. p. 229-237.
77. K. Miyamoto, H. Takiwaki, G. G. Hillebrand and S. Arase, "Development of a digital imaging system for objective measurement of hyperpigmented spots on the face", *Skin Research and Technology*, 8(4), 227-235, 2002.
78. W. Westerhof, "CIE Colorimetry", in *Handbook of non-invasive methods and the skin*, J. Serup and G. B. E. Jemec, eds. 1995, CRC Press: Boca Raton. p. 385-397.

79. R. Breit, H. Kleber and W. Will, "Measurement of erythema response to ultraviolet radiation by "monochromatic" photography", *Archives of Dermatological Research*, 272(1-2), 93-96, 1982.
80. S. Arai, "Analysis of Pigmentation of Human Skin (UV-Light Images)", in *Bioengineering of the skin : skin surface imaging and analysis*, K.-P. Wilhelm, P. Elsner, E. Berardesca and H. I. Maibach, eds. 1997, CRC Press: Boca Raton. p. 85-94.
81. R. R. Anderson, "Polarized-Light Examination and Photography of the Skin", *Archives of Dermatology*, 127(7), 1000-1005, 1991.
82. J. O'Doherty, J. Henricson, C. Anderson, M. J. Leahy, G. E. Nilsson and F. Sjoberg, "Sub-epidermal imaging using polarized light spectroscopy for assessment of skin microcirculation", *Skin Research and Technology*, 13(4), 472-484, 2007.
83. G. B. E. Jemec and J. Serup, *Handbook of non-invasive methods and the skin*, pp. 702, CRC Press, Boca Raton, 1995.
84. A. D. Pearse, C. Edwards, S. Hill and R. Marks, "Portable Erythema Meter and Its Application to Use in Human Skin", *International Journal of Cosmetic Science*, 12(2), 63-70, 1990.
85. I. L. Weatherall and B. D. Coombs, "Skin Color Measurements in Terms of Cielab Color Space Values", *Journal of Investigative Dermatology*, 99(4), 468-473, 1992.
86. R. R. Anderson and J. A. Parrish, "Optical Properties of Human Skin", in *The Science of Photomedicine*, J. D. Regan and J. A. Parrish, eds. 1982, Plenum Press: New York. p. 147-194.
87. S. L. Jacques and B. W. Pogue, "Tutorial on Diffuse Light Transport", *Journal of Biomedical Optics*, 13(4), -, 2008.
88. W. F. Cheong, S. A. Prahl and A. J. Welch, "A Review of the Optical-Properties of Biological Tissues", *IEEE Journal of Quantum Electronics*, 26(12), 2166-2185, 1990.
89. M. Larsson, *Influence of optical properties on Laser Doppler Flowmetry*, pp. 64, University of Linköping, Linköping, 2004.
90. Y. Tsuchiya, "Photon path distribution and optical responses of turbid media: theoretical analysis based on the microscopic Beer-Lambert law", *Physics in Medicine and Biology*, 46(8), 2067-2084, 2001.
91. F. A. Duck, *Physical properties of tissue : a comprehensive reference book*, pp. 346, Academic P., London, 1990.
92. M. Friebel and M. Meinke, "Determination of the complex refractive index of highly concentrated hemoglobin solutions using transmittance and reflectance measurements", *Journal of Biomedical Optics*, 10(6), -, 2005.
93. V. Tuchin, *Tissue optics : light scattering methods and instruments for medical diagnosis*, pp. 352, SPIE Optical Engineering Press, Bellingham, Wash, 2000.
94. D. J. Faber, M. C. G. Aalders, E. G. Mik, B. A. Hooper, M. J. C. van Gemert and T. G. van Leeuwen, "Oxygen saturation-dependent absorption and scattering of blood", *Physical Review Letters*, 93(2), -, 2004.
95. L. H. Kou, D. Labrie and P. Chylek, "Refractive-Indexes of Water and Ice in the 0.65-Mu-M to 2.5-Mu-M Spectral Range", *Applied Optics*, 32(19), 3531-3540, 1993.
96. E. Hecht, *Optics*, pp. 698, Addison Wesley, San Francisco, 2002.
97. V. V. Tuchin, "Light scattering study of tissues", *Uspekhi Fizicheskikh Nauk*, 40(5), 495-515, 1997.
98. R. R. Anderson and J. A. Parrish, "The optics of human skin", *The Journal of Investigative Dermatology*, 77(1), 13-19, 1981.
99. B. C. Wilson and S. L. Jacques, "Optical Reflectance and Transmittance of Tissues - Principles and Applications", *IEEE Journal of Quantum Electronics*, 26(12), 2186-2199, 1990.

100. I. E. Kochevar, M. A. Pathak and J. A. Parrish, "Photophysics, Photochemistry, and Photobiology", in *Fitzpatrick's dermatology in general medicine*, I. M. Freedberg, A. Z. Eisen, K. Wolff, K. F. Austen, L. A. Goldsmith, I. S. Katz and T. B. Fitzpatrick, eds. 1999, McGraw-Hill: New York; London. p. 220-229.
101. T. J. Dougherty and J. G. Levy, "Photodynamic Therapy (PDT) and Clinical Applications", in *Biomedical photonics handbook*, T. Vo-Dinh, ed. 2003, CRC Press: Boca Raton, Fla. p. 6-1-6-30.
102. L. V. Wang and H.-i. Wu, *Biomedical optics : principles and imaging*, pp. 362, Wiley-Interscience, Hoboken, N.J., 2007.
103. W. G. Zijlstra, A. Buursma and O. W. van Assendelft, *Visible and Near Infrared Absorption Spectra of Human and Animal Haemoglobin*, pp. 368, VSP BV, Leiden, The Netherlands, 2000.
104. J. R. Mourant, J. Boyer, A. H. Hielscher and I. J. Bigio, "Influence of the scattering phase function on light transport measurements in turbid media performed with small source-detector separations", *Optics Letters*, 21(7), 546-548, 1996.
105. S. Prahl, *Optical Absorption of Hemoglobin*, <http://omlc.ogi.edu/spectra/hemoglobin/index.html>, Last access: November, 2007.
106. W. G. Zijlstra, A. Buursma and O. W. Van Assendelft, *Visible and Near Infrared Absorption Spectra of Human and Animal Haemoglobin: Determination and Application*, pp. 368, VSP, Utrecht, 2000.
107. L. L. Randeberg, O. A. Haugen, R. Haaverstad and L. O. Svaasand, "A novel approach to age determination of traumatic injuries by reflectance spectroscopy", *Lasers in Surgery and Medicine*, 38(4), 277-289, 2006.
108. G. A. Ordway and D. J. Garry, "Myoglobin: an essential hemoprotein in striated muscle", *Journal of Experimental Biology*, 207(20), 3441-3446, 2004.
109. K. A. Schenkman, D. R. Marble, D. H. Burns and E. O. Feigl, "Myoglobin oxygen dissociation by multiwavelength spectroscopy", *Journal of Applied Physiology*, 82(1), 86-92, 1997.
110. L. Eddy, A. Arduini and P. Hochstein, "Reduction of Ferrylmyoglobin in Rat Diaphragm", *American Journal of Physiology*, 259(6), C995-C997, 1990.
111. F. F. Jöbssis-VanderVliet, C. A. Piantadosi, A. L. Sylvia, S. K. Lucas and H. H. Keizer, "Near-infrared monitoring of cerebral oxygen sufficiency. I. Spectra of cytochrome c oxidase", *Neurological Research*, 10(1), 7-17, 1988.
112. C. E. Cooper, M. Cope, V. Quaresima, M. Ferrari, E. Nemoto, R. Springett, S. Matcher, P. Amess, J. Penrice, L. Tyszczuk, J. Wyatt and D. T. Delpy, "Measurement of cytochrome oxidase redox state by near infrared spectroscopy", *Optical Imaging of Brain Function and Metabolism 2*, 413, 63-73, 1997.
113. B. O. R. Laboratory, *Specific Extinction Spectra of Tissue Chromophores*, http://www.medphys.ucl.ac.uk/research/borl/research/NIR_topics/spectra/spectra.htm, Last access: June, 2008.
114. U. Heinrich, *Untersuchungen zur quantitativen photometrischen Analyse der Redox-Zustände der Atmungskette in vitro und in vivo am Beispiel des Gehirns*, in *Abteilung für Biologie*, Ruhr-Universität Bochum: Bochum. p. 122. 1981.
115. L. L. Randeberg, *Diagnostic applications of diffuse reflectance spectroscopy*, in *Faculty of Information Technology Mathematics and Electrical Engineering Department of Electronics and Telecommunications*, Norwegian University of Science and Technology: Trondheim. p. 48. 2005.
116. J. M. Dixon, M. Taniguchi and J. S. Lindsey, "PhotochemCAD 2: A refined program with accompanying spectral databases for photochemical calculations", *Photochemistry and Photobiology*, 81(1), 212-213, 2005.
117. I. M. Freedberg and T. B. Fitzpatrick, *Fitzpatrick's dermatology in general medicine*, pp. 1659, 1999.

118. N. G. Jablonski, "The evolution of human skin and skin color", *Annual Review of Anthropology*, 33, 585-623, 2004.
119. A. J. Thody, E. M. Higgins, K. Wakamatsu, S. Ito, S. A. Burchill and J. M. Marks, "Pheomelanin as well as eumelanin is present in human epidermis", *Journal of Investigative Dermatology*, 97(2), 340-344, 1991.
120. S. L. Jacques, *Extinction coefficient of melanin*, <http://omlc.ogi.edu/spectra/melanin/eumelanin.html>, Last access: January, 2007.
121. B. A. Gilchrist, "Actinic Injury", *Annual Review of Medicine*, 41, 199-210, 1990.
122. H. Hönigsmann, "Erythema and pigmentation", *Photodermatology Photoimmunology & Photomedicine*, 18(2), 75-81, 2002.
123. M. L. Wolbarsht, A. W. Walsh and G. George, "Melanin, a unique absorber", *Applied Optics*, 20(13), 2184-2186, 1981.
124. G. Britton, "Structure and properties of carotenoids in relation to function", *The FASEB Journal*, 9(15), 1551-1558, 1995.
125. H. K. Biesalski and U. C. Obermueller-Jevic, "UV light, beta-carotene and human skin - Beneficial and potentially harmful effects", *Archives of Biochemistry and Biophysics*, 389(1), 1-6, 2001.
126. U. Heinrich, C. Gartner, M. Wiebusch, O. Eichler, H. Sies, H. Tronnier and W. Stahl, "Supplementation with beta-carotene or a similar amount of mixed carotenoids protects humans from UV-induced erythema", *The Journal of Nutrition*, 133(1), 98-101, 2003.
127. A. Junghans, H. Sies and W. Stahl, "Macular pigments lutein and zeaxanthin as blue light filters studied in liposomes", *Archives of Biochemistry and Biophysics*, 391(2), 160-164, 2001.
128. R. L. P. van Veen, H. J. C. M. Sterenborg, A. Pifferi, A. Torricelli, E. Chikoidze and R. Cubeddu, "Determination of visible near-IR absorption coefficients of mammalian fat using time- and spatially resolved diffuse reflectance and transmission spectroscopy", *Journal of Biomedical Optics*, 10(5), 054004, 2005.
129. H. Q. Woodard and D. R. White, "The Composition of Body-Tissues", *British Journal of Radiology*, 59(708), 1209-1219, 1986.
130. D. Segelstein, *The complex refractive index of water*, in, University of Missouri: Kansas City. p. 1981.
131. S. A. Prahl, *Optical Absorption of Fat*, <http://omlc.ogi.edu/spectra/fat/>, Last access: June, 2007.
132. S. A. Prahl, *Optical Absorption of Water Compendium*, <http://omlc.ogi.edu/spectra/water/abs/index.html>, Last access: June, 2007.
133. K. Nassau, *The physics and chemistry of color: the fifteen causes of color*, pp. 481, Wiley, New York, 2001.
134. G. Goerz, A. Link-Mannhardt, K. Bolsen, M. Zumdick, C. Fritsch and N. V. Schürer, "Porphyrin concentrations in various human tissues." *Experimental Dermatology*, 4, 218-220, 1995.
135. S. Andersson-Engels, C. Klinteberg, K. Svanberg and S. Svanberg, "In vivo fluorescence imaging for tissue diagnostics", *Physics in Medicine and Biology*, 42(5), 815-824, 1997.
136. A. Caggiati, C. Rosi, M. Franceschini and D. Innocenzi, "The nature of skin pigmentations in chronic venous insufficiency: A preliminary report", *European Journal of Vascular and Endovascular Surgery*, 35(1), 111-118, 2008.
137. W. Chua-anusorn, K. C. Tran, J. Webb, D. J. Macey and T. G. St Pierre, "Chemical speciation of iron deposits in thalassemic heart tissue", *Inorganica Chimica Acta*, 300, 932-936, 2000.
138. A. R. Young, "Chromophores in human skin", *Physics in Medicine and Biology*, 42(5), 789-802, 1997.

139. M. Shimada, Y. Masuda, Y. Yamada, M. Itoh, M. Takahashi and T. Yatagai, "Explanation of human skin color by multiple linear regression analysis based on the modified Lambert-Beer law", *Optical Review*, 7(4), 348-352, 2000.
140. S. R. Arridge, M. Cope and D. T. Delpy, "The theoretical basis for the determination of optical pathlengths in tissue: temporal and frequency analysis", *Physics in Medicine and Biology*, 37(7), 1531-1560, 1992.
141. A. Sassaroli and S. Fantini, "Comment on the modified Beer-Lambert law for scattering media", *Physics in Medicine and Biology*, 49(14), N255-N257, 2004.
142. D. T. Delpy, M. Cope, P. Vanderzee, S. Arridge, S. Wray and J. Wyatt, "Estimation of Optical Pathlength through Tissue from Direct Time of Flight Measurement", *Physics in Medicine and Biology*, 33(12), 1433-1442, 1988.
143. M. Hiraoka, M. Firbank, M. Essenpreis, M. Cope, S. R. Arridge, P. Vanderzee and D. T. Delpy, "A Monte-Carlo Investigation of Optical Pathlength in Inhomogeneous Tissue and Its Application to near-Infrared Spectroscopy", *Physics in Medicine and Biology*, 38(12), 1859-1876, 1993.
144. M. Shimada, Y. Yamada, M. Itoh and T. Yatagai, "Melanin and blood concentration in a human skin model studied by multiple regression analysis: assessment by Monte Carlo simulation", *Physics in Medicine and Biology*, 46(9), 2397-2406, 2001.
145. S. L. Jacques, P. R. Bargo and K. Engelking, *Optical fiber reflectance spectroscopy*, Saratov Fall Meeting, <http://omlc.ogi.edu/news/oct03/saratov/index.htm>, Last access: April 25, 2007.
146. S. L. Jacques, P. Bargo and K. Engelking, *Optical fiber reflectance spectroscopy*, Saratov Fall Meeting 2003, <http://omlc.ogi.edu/news/oct03/saratov/index.htm>, Last access: January, 2007.
147. A. M. K. Nilsson, C. Stureson, D. L. Liu and S. Andersson-Engels, "Changes in spectral shape of tissue optical properties in conjunction with laser-induced thermotherapy", *Applied Optics*, 37(7), 1256-1267, 1998.
148. D. W. Marquardt, "An Algorithm for Least-Squares Estimation of Nonlinear Parameters", *Journal of the Society for Industrial and Applied Mathematics*, 11(2), 431-441, 1963.
149. D. C. Montgomery and G. C. Runger, "Multiple Linear Regression", in *Applied Statistics and Probability for Engineers*, 1994, Wiley: New York. p. 531-624.
150. E. W. Weisstein, *Correlation Coefficient*, From MathWorld - A Wolfram Web Resource, <http://mathworld.wolfram.com/CorrelationCoefficient.html>, Last access: October, 2008.
151. G. N. Stamatas and N. Kollias. *Noninvasive quantitative documentation of cutaneous inflammation in vivo using spectral imaging*. in *Photonic Therapeutics and Diagnostics II*. 2006. San Jose, USA: Proceedings of SPIE.
152. G. N. Stamatas and N. Kollias, "In vivo documentation of cutaneous inflammation using spectral imaging", *Journal of Biomedical Optics*, 12(5), 051603, 2007.
153. S. P. Nighswander-Rempel, R. A. Shaw, V. V. Kupriyanov, J. Rendell, B. Xiang and H. Mantsch, "Mapping tissue oxygenation in the beating heart with near-infrared spectroscopic imaging", *Vibrational Spectroscopy*, 32(1), 85-94, 2003.
154. L. Martinez. *A non-invasive spectral reflectance method for mapping blood oxygen saturation in wounds*. in 31st Applied Imagery Pattern Recognition Workshop. 2002. Washington, D.C., USA: IEEE Computer Society.
155. L. L. Randeberg, A. M. Winnem, N. E. Langlois, E. L. P. Larsen, R. Haaverstad, B. Skallerud, O. A. Haugen and L. O. Svaasand, "Skin changes following minor trauma", *Lasers in Surgery and Medicine*, 39(5), 403-413, 2007.
156. S. G. Kong, M. E. Martin and T. Vo-Dinh, "Hyperspectral fluorescence imaging for mouse skin tumor detection", *Etri Journal*, 28(6), 770-776, 2006.

157. G. Bearman and R. Levenson, "Biological Imaging Spectroscopy", in *Biomedical photonics handbook*, T. Vo-Dinh, ed. 2003, CRC Press: Boca Raton, Fla. p. 8-1-8-26.
158. R. Gillies, J. E. Freeman, L. C. Cancio, D. Brand, M. Hopmeier and J. R. Mansfield, "Systemic effects of shock and resuscitation monitored by visible hyperspectral imaging", *Diabetes Technology & Therapeutics*, 5(5), 847-855, 2003.
159. L. C. Cancio, A. I. Batchinsky, J. R. Mansfield, S. Panasyuk, K. Hetz, D. Martini, B. S. Jordan, B. Tracey and J. E. Freeman, "Hyperspectral imaging: a new approach to the diagnosis of hemorrhagic shock", *The Journal of Trauma*, 60(5), 1087-1095, 2006.
160. M. Arildsson, C. L. Asker, E. G. Salerud and T. Stromberg, "Skin capillary appearance and skin microvascular perfusion due to topical application of analgesia cream", *Microvascular Research*, 59(1), 14-23, 2000.
161. M. Arildsson, G. E. Nilsson and T. Strömberg, "Effects on skin blood flow by provocation during local analgesia", *Microvascular Research*, 59(1), 122-130, 2000.
162. N. Kollias and A. H. Baqer, "Quantitative assessment of UV-induced pigmentation and erythema", *Photo-dermatology*, 5(1), 53-60, 1988.
163. S. L. Jacques and D. J. McAuliffe, "The melanosome: threshold temperature for explosive vaporization and internal absorption coefficient during pulsed laser irradiation", *Photochemistry and Photobiology*, 53(6), 769-775, 1991.
164. M. A. Ilias, *Single exposure phototesting and assessment of pigmented skin lesions : quantitative methods in terms of blood perfusion estimates*, pp. 68, University of Linköping, Linköping, 2003.
165. N. Kollias, A. Baqer and I. Sadiq, "Minimum erythema dose determination in individuals of skin type V and VI with diffuse reflectance spectroscopy", *Photodermatology, Photoimmunology & Photomedicine*, 10(6), 249-254, 1994.
166. I. V. Meglinski and S. J. Matcher, "Modelling the sampling volume for skin blood oxygenation measurements", *Medical & Biological Engineering & Computing*, 39(1), 44-50, 2001.
167. J. R. Mourant, I. J. Bigio, D. A. Jack, T. M. Johnson and H. D. Miller, "Measuring absorption coefficients in small volumes of highly scattering media: Source-detector separations for which path lengths do not depend on scattering properties", *Applied Optics*, 36(22), 5655-5661, 1997.
168. M. Larsson, H. Nilsson and T. Stromberg, "In vivo determination of local skin optical properties and photon path length by use of spatially resolved diffuse reflectance with applications in laser Doppler flowmetry", *Applied Optics*, 42(1), 124-134, 2003.
169. A. Amelink, H. J. C. M. Sterenberg, M. P. L. Bard and S. A. Burgers, "In vivo measurement of the local optical properties of tissue by use of differential path-length spectroscopy", *Optics Letters*, 29(10), 1087-1089, 2004.
170. J. C. Finlay and T. H. Foster, "Hemoglobin oxygen saturations in phantoms and in vivo from measurements of steady-state diffuse reflectance at a single, short source-detector separation", *Medical Physics*, 31(7), 1949-1959, 2004.
171. L. S. L. Arakaki, M. J. Kushmerick and D. H. Burns, "Myoglobin oxygen saturation measured independently of hemoglobin in scattering media by optical reflectance spectroscopy", *Applied Spectroscopy*, 50(6), 697-707, 1996.
172. A. E. Arai, C. E. Kasserra, P. R. Territo, A. H. Gandjbakhche and R. S. Balaban, "Myocardial oxygenation in vivo: optical spectroscopy of cytoplasmic myoglobin and mitochondrial cytochromes", *American Journal of Physiology-Heart and Circulatory Physiology*, 277(2), H683-H697, 1999.
173. K. A. Schenkman, D. R. Marble, E. O. Feigl and D. H. Burns, "Near-infrared spectroscopic measurement of myoglobin oxygen saturation in the presence of hemoglobin using partial least-squares analysis", *Applied Spectroscopy*, 53(3), 325-331, 1999.

174. C. Mork, K. Kvernebo, C. L. Asker and E. G. Salerud, "Reduced skin capillary density during attacks of erythromelalgia implies arteriovenous shunting as pathogenetic mechanism", *Journal of Investigative Dermatology*, 119(4), 949-953, 2002.
175. A. Korzon-Burakowska and M. Edmonds, "Role of the microcirculation in diabetic foot ulceration", *The International Journal of Lower Extremity Wounds*, 5(3), 144-148, 2006.
176. K. J. Zuzak, M. D. Schaeberle, E. N. Lewis and I. W. Levin, "Visible reflectance hyperspectral imaging: characterization of a noninvasive, in vivo system for determining tissue perfusion", *Analytical Chemistry*, 74(9), 2021-2028, 2002.
177. N. Kollias, R. Gillies, J. A. Muccini, R. K. Uyeyama, S. B. Phillips and L. A. Drake, "A Single-Parameter, Oxygenated Hemoglobin, Can Be Used to Quantify Experimental Irritant-Induced Inflammation", *Journal of Investigative Dermatology*, 104(3), 421-424, 1995.